https://doi.org/10.5194/egusphere-2026-1900
Preprint. Discussion started: 19 June 2026

Evaluation of WRF-Chem (version 4.7.1) aeolian dust emission and land surface models over the dust belt

Semontee Deb[1], Elena Louca[1], Angelos Violaris[1], Pantelis Kiriakidis[1], Yiannis Proestos[1], Jonilda Kushta[1,*], Antonis Gkikas[2], Andrea Pozzer[3,1], and Theodoros Christoudias[1]

[1]Climate & Atmosphere Research Centre, The Cyprus Institute, Nicosia, Cyprus
[2]Academy of Athens, Greece
[3]Atmospheric Chemistry Department, Max Planck Institute for Chemistry, Mainz, Germany
[*]now at the European Centre for Medium-Range Weather Forecasts (ECMWF), Bonn, Germany

Correspondence: Theodoros Christoudias (t.christoudias@cyi.ac.cy)

Abstract. Aeolian dust is a key component of the Earth system, influencing biogeochemical cycles, cloud microphysics, and the radiative energy budget and atmospheric dynamics, while also degrading air quality around major source regions. Simulating mineral dust remains a major challenge for regional and global atmospheric models due to uncertainties in emission processes, land-surface interactions, together with limited availability of observations. In this study, we present the first comprehensive, year-long evaluation of the simulated dust with the WRF-Chem model (v4.7.1) over the dust belt spanning North Africa, the Middle East, and Central Asia. We evaluate an ensemble of six simulations using three widely applied dust emission schemes (GOCART, GOCART-AFWA, and University of Cologne – UoC) combined with two advanced land surface models (LSM): Noah-MP and CLM4. The model performance is evaluated through a set of observations, including the MODIS-derived MIDAS dust optical depth product, AERONET aerosol optical depth (AOD), ERA5-Land surface soil moisture and wind speed, and EMEP coarse particulate matter (PM_{10}-$PM_{2.5}$) measurements. We find that among the dust emission schemes, GOCART provides the most robust agreement with MIDAS and AERONET, closely followed by AFWA but with a wider spread, while UoC systematically diverges from observations failing to represent realistic column dust optical depth. Evaluation of surface drivers reveals that land-surface representation exerts a strong influence on dust emission magnitude and spatial distribution, with Noah-MP yielding systematically better agreement with observed meteorology and AOD, whereas CLM4 introduces more pronounced regional discrepancies. UoC exhibits improved alignment with coarse particulate matter measurements at the EMEP stations compared to GOCART and AFWA. Finally, we provide empirical scaling factors derived for each emissions mechanism–LSM pairing, applicable for WRF-Chem dust simulations, offering guidance for improved dust and air quality, and climate modelling applications.

1 Introduction

The dust belt, the continental zone of arid and semi-arid lands stretching from the Sahel across North Africa, the Middle East, and Central Asia, to the Gobi Desert, is known for frequent and severe dust storms and is the major source of atmospheric dust, contributing with more than 85% of the total dust load worldwide (Kok et al., 2021b). Aeolian dust is an essential component of

https://doi.org/10.5194/egusphere-2026-1900
Preprint. Discussion started: 19 June 2026

the earth's atmosphere and plays a fundamental part in climate dynamics, critical for the model representation of hydrological cycles (Miller et al., 2004; Mahowald et al., 2010), biogeochemistry, oceanic eutrophication, and economic and human health impacts (Prospero et al., 2002; Griffin, 2007; Giannadaki et al., 2014; Zhang et al., 2016). However, the global dust emission flux, mostly originating from the dust belt, is highly uncertain; estimated to be in the range of 1000 and 5000 $\mathrm{Tg/y}$ (Kok et al., 2021a). Thus, the dust emission flux in atmospheric/climate models is typically adjusted by empirical scaling factors (Zhao et al., 2022). Incorporating the emission of mineral dust into atmospheric models presents challenges due to the complexity of emission processes over multiple scales, and atmosphere-land interactions (Tegen and Fung, 1994; Pérez et al., 2006).

Land surface models (LSMs) in particular play a pivotal role in simulating aeolian dust emissions within atmospheric models, as they provide the key relevant surface and soil variables that directly influence emissions. Through the representation of soil moisture, surface temperature and roughness, vegetation cover, and snow or ice fraction, LSMs determine the erodibility and aerodynamic conditions of the land surface that feed directly into the dust emission parameterisations. They also provide models with surface fluxes of momentum, heat, and moisture, influencing near-surface wind fields and boundary-layer turbulence that drive dust mobilization. Consequently, it can be expected that the accuracy of dust emission estimates and their temporal variability strongly depend on the choice of LSM.

A number of studies in the literature aimed to evaluate the skill of the weather research and forecast with chemistry community model WRF-Chem (Grell et al., 2005) in simulating aeolian dust, using different coupled dust emission schemes: the GOCART scheme, based on the Goddard Chemistry Aerosol Radiation and Transport (GOCART) model (Ginoux et al., 2001), the Air Force Weather Agency dust emission scheme (AFWA) for the GOCART aerosol model (LeGrand et al., 2019) and the University of Cologne (UoC) parameterisation (Shao, 2001, 2004; Shao et al., 2011, referred to as UoC01, UoC04, UoC11 respectively). Chen et al. (2013) implemented the WRF-Chem model to model dust emission and transport during an intense dust storm event over Asia. The model captured the geographical distribution of satellite-derived aerosol optical depth (AOD) over the Taklimakan desert, suggesting that the GOCART scheme effectively represents the dust source region in this area. The results were also validated against MODIS, MISR, and CALIPSO satellite AOD retrievals. Flaounas et al. (2017) evaluated the efficiency of the different dust emission parameterizations within WRF-Chem version 3.6.1 over the greater Mediterranean region for a period of six months, spanning the spring and summer seasons of 2011. However, they do not report the LSM used. The AFWA and the UoC dust schemes were further subjected to a study in 2016 over the Middle Eastern region during the summer period (Fountoukis et al., 2016). The study identified significant discrepancies for both schemes in comparison to in-situ measurements. Over the Arabian Peninsula, the AFWA scheme was found to yield dust emission fluxes 30% greater than those produced by the UoC. Sensitivity analysis of WRF-Chem conducted for dust events in China during May 2018 by Zhao et al. (2020), and a 2015 winter-time dust event in East Asia (Lee and Lee, 2022), outlined the lack of ability of the UoC scheme to properly simulate dust processes for this region. Yuan et al. (2019) evaluated the GOCART, AFWA and UoC schemes in WRF-Chem for a singular dust event in Central Asia. All three schemes showed good agreement with satellite measurements, however, the GOCART and AFWA schemes overestimate AOD over Iran. Najafpour et al. (2023) presented a similar evaluation of dust emissions integrated in the WRF-Chem model over Iran, and inferred the suitability of the GOCART,

https://doi.org/10.5194/egusphere-2026-1900
Preprint. Discussion started: 19 June 2026

followed by the AFWA scheme for this region. In all instances, the authors did not evaluate the impact on the model skill of the choice of LSM.

To our knowledge, the studies that evaluated the impact of different LSMs (Sec. 2.2) were limited to single episodes or events, over limited areas, and simulated a single season at most. Su and Fung (2015) modelled springtime dust cycles in 2006 over East Asia employing AFWA and UoC dust emission algorithms with the Noah LSM model that has since been superseded by the Noah-MP model (Sec. 2.2), and soil map from the United States Geological Survey (USGS). They performed another experiment with UoC and Beijing Normal University (BNU) soil data. Model evaluation in both cases revealed that UoC exhibited better agreement for surface coarse particulate matter up to $10\,\mu\mathrm{m}$ (PM_{10}) concentrations. However, there were several inconsistencies in model performance between the two cases, in particular arising from the underestimation of dust emission by the AFWA scheme. Rizza et al. (2018) assessed the effectiveness of WRF-Chem model using different land surface schemes coupled with UoC dust emissions to examine a dust episode across the Central Mediterranean region. The analysis revealed that pairing the dust scheme with the Noah or Noah-MP LSM yielded improved results, particularly for daily averaged PM_{10}. Finally, Yoon et al. (2025) recently assessed the simulation capability of WRF-Chem for different configurations of four land surface, and five dust emission schemes over Asia. The study identified the combination of UoC04-CLM4 dust and land surface scheme to outperform the other scheme combinations, closely matched by UoC01.

A comprehensive evaluation of the dust scheme in WRF-Chem over extended periods is lacking in the literature, highlighting the need for an in-depth investigation across a broader domain that captures multiple events throughout the year. This paper provides a year-round, detailed evaluation of WRF-Chem simulations using multiple dust emissions and land surface model combinations, over the whole dust belt, covering North Africa, Middle East and the Arabian Peninsula, and adjacent receptor regions, uniquely offering broader insight into model performance, beyond event-specific or region-limited analyses. We evaluate the model against satellite-derived products over the whole emission domain, and determine the values for the empirical emissions scale factors that are applicable in the broader spatio-temporal domain affected by the dust belt. Finally, we validate the model simulations over receptor regions with dense observation station networks in continental Europe and Middle East and the extended Mediterranean basin.

2 WRF-Chem model configuration

We use the Weather Research and Forecasting model with integrated Chemistry WRF-Chem version 4.7.1 (Grell et al., 2005). Our simulations are performed over a full calendar year from 1st January to 31st December 2021, following one month of spin-up (December 2020). The model is initialised and driven at the boundaries by meteorological fields which are provided by the global final analysis (FNL), produced by the Global Forecast System (GFS) of the National Centers for Environmental Prediction (NCEP) in $0.25^\circ \times 0.25^\circ$ resolution. The meteorological boundary conditions are updated every 3 hours, and the model horizontal wind components, temperature and humidity are nudged at every time-step towards six-hourly reanalysis data with a relaxation coefficient of $3 \times 10^{-4}\ \mathrm{s}^{-1}$ (with no ramping).

https://doi.org/10.5194/egusphere-2026-1900
Preprint. Discussion started: 19 June 2026

The simulation domain at 50 km horizontal resolution (155×105 grid-points) and 33 vertical layers up to 50 hPa inlcudes a broad region that encompasses the "dust belt", the band of areas around the globe with significant dust sources, primarily located in North Africa, the Middle East, and western and parts of central Asia (Fig. 1). These regions are major contributors to global dust emissions and are linked by atmospheric circulation patterns. Our simulation domain also includes the Mediterranean basin and continental Europe, receptor regions of aeolian dust with available measurements from dense observation station networks.

For our study, model physics parameterisations follow the optimal configuration following Georgiou et al. (2022) that was demonstrated to most accurately reproduce meteorological parameters, including total precipitation and air temperature over the Middle East – North Africa CORDEX domain (Zittis et al., 2014). We use the Grell-Freitas cumulus parametrisation scheme for convection (Freitas et al., 2021), the Yonsei University (Hong et al., 2006) planetary boundary layer (PBL), and the Rapid Radiative Transfer Model (RRTMG) Longwave and Shortwave Radation (Mlawer et al., 1997) with dust-aerosol feedbacks. The simulations use the five-bin dust and four-bin sea salt mechanism within the GOCART aerosol scheme (`chem_opt=300`, Chin et al., 2000). The emissions of seal salt are computed online at runtime.

As dust simulations are heavily influenced by both dust emission schemes and land surface models (Yoon et al., 2025; Bukowski and van den Heever, 2022), it is imperative to evaluate their combined performance on model dust emission, transport and aerosol-radiation feedbacks to better understand model sensitivity and improve predictive accuracy. For our analysis we have produced a cohort of simulations with all combinations of the three dust emission and two state-of-the-art land surface schemes within WRF-Chem, as presented in the next sections.

2.1 Dust emission algorithms

The basic mechanisms for the three WRF-CHEM dust emission schemes considered (GOCART, AFWA, UoC) are given below, and the readers can find all details in references therein:

GOCART The Goddard Chemistry Aerosol Radiation and Transport (GOCART) model (Chin et al., 2000) was modified with a dust source function by Ginoux et al. (2001), leading to an initial reproduction of global dust loadings by simulating dust emissions, transport, and removal processes based on topographic source identification. The GOCART emission scheme is based on the empirical expression by Gillette and Passi (1988) that uses the surface wind speed compared to the erosive wind speed threshold, and soil wetness to calculate the dust emission flux F_p (Chin et al., 2000; Ginoux et al., 2001), distributing the emissions across particle size sections (bins) ranging from 0.1 to 10 µm in diameter to represent the dust aerosol size spectrum:

$$F_p = \begin{cases} CSs_p u_{10\mathrm{m}}^2 (u_{10\mathrm{m}} - u_t), & \text{if } u_{10\mathrm{m}} > u_t \\ 0, & \text{otherwise} \end{cases}$$

where C is an empirical constant derived by Ginoux et al. (2001), S is a function of erodibility for identifying dust source regions, s_p gives the fraction for each size sections, u_{10m} and u_t are the horizontal wind speed at 10 m and threshold wind velocity respectively.

https://doi.org/10.5194/egusphere-2026-1900
Preprint. Discussion started: 19 June 2026

AFWA This is an extention of the GOCART scheme by the Air Force Weather Agency (AFWA) (LeGrand et al., 2019) to represent saltation bombardment. The AFWA dust module is primarily founded on the dust emission function by Marticorena and Bergametti (1995), which considers saltation of dust particles (LeGrand et al., 2019). In this scheme the dust emission is simulated as a two-stage process which involves the wind-shear triggering the saltation of large particles, followed by emission of finer particles. The saltation flux Q is expressed as follows:

$$Q = C_{mb}\frac{\rho_a}{g}u_*^3\left(1+\frac{u_{*t}}{u_*}\right)\left(1-\frac{u_{*t}^2}{u_*^2}\right), \quad u_* \geq u_{*t}$$

where C_{mb} is a scaling constant for emission, ρ_a is the density of air, g is gravitational acceleration, and u_t and u_{*t} correspond to friction velocity and its threshold. The total horizontal saltation flux is given by the expression:

$$G = \sum_s Q(D_s)\,\mathrm{d}S_{\mathrm{rel}}(D_s)$$

$$F_{bulk} = G\alpha \times S$$

where S is the erodibility factor, F_{bulk} is the dust flux of the vertical column and α is the factor of bombardment efficiency (Gillett and Morales, 1979). The AFWA dust emission scheme for the GOCART aerosol model was documented in LeGrand et al. (2019) and the scheme was tested for a dust event in southwest Asia. They indicated that the AFWA scheme may better capture mesoscale features due to reduced sensitivity to limited soil and vegetation data.

UoC Shao (2001) developed a dust emission model that incorporates saltation bombardment and disintegration of soil aggregates, known as the University of Cologne (UoC) scheme. This was later simplified (Shao, 2004) to improve the computational efficiency, and further refined (Shao et al., 2011). It calculates the vertical flux of dust taking into account the saltation bombardment and aggregate disintegration of particles which is given by:

$$F(d_i, d_s) = c_y\left[(1-\gamma)+\gamma\frac{p_m(d_i)}{p_f(d_i)}\right]\frac{Q_{d_s}g}{u_*^2 m}\left(\rho_b\eta_{fi}\Omega+\eta_{cl}m\right)$$

where γ denotes the size distribution weight factor for dust particles, m is the mass, g is the gravitational acceleration, d_i is the size of the particle produced due to saltation of particle of size d_s, u_* is the friction velocity, $p_m(d_i)$ and $p_f(d_i)$ are minimally and fully dispersed size distribution of particles; ρ_b is the soil particle density, Ω denotes the total volume of soil displaced by the particle due to bombardment based on the swept area and the contact width, η_{fi} and η_{ci} represent the mass fraction for contained dust and aggregated dust respectively, and Q_{d_s} is the saltation flux. The initial scheme (Shao, 2001) was enhanced for computational efficiency (Shao, 2004) followed by further simplification (Shao et al., 2011). In terms of the representation of dust loading and transport, both UoC01 (Shao, 2001) and UoC04 Shao (2004) were shown to have closely resembling patterns when compared with observations, while UoC04 is using a computationally more efficient parameterisation. UoC11 was found to be unable to reproduce observed dust loading substantially (Yoon et al., 2025). Therefore, for this study we use the simplified form UoC04, (Shao, 2004), henceforth

https://doi.org/10.5194/egusphere-2026-1900
Preprint. Discussion started: 19 June 2026

referred to as UoC, with the dust emission flux given by:

$$F(d_i, d_s) = c_y \eta_{fi} \left[(1-\gamma) + \gamma \sigma_p\right] \frac{Q_{d_s} g}{u_*^2} (1 + \sigma_m)$$

$$\sigma_p = \frac{p_m(d_i)}{p_f(d_i)}$$

where σ_p represents the mass ratio between free dust particles and aggregated dust, while σ_m denotes the efficiency of particle bombardment.

All dust emission schemes use as input from the WRF-CHEM pre-processor the erodible fraction field, a map representing the proportion of each grid cell susceptible to wind erosion for different soil classes (sand, silt, and clay), as shown in Fig.1. In the GOCART and AFWA schemes, this field is used a proportionality factor for the emission flux (LeGrand et al., 2019). In the UoC scheme it represents the availability of erodible material at the surface, and thus only acts as a threshold condition for dust emission (Shao, 2001).

2.2 Land surface models

In this work we evaluate, in combination with the dust emissions algorithms, the Noah-Multiparameterization Land Surface Model (Noah-MP LSM) version 5.0 (He et al., 2023), and the Community Land Model (CLM) version 4 (Lawrence et al., 2011).

Noah-MP The Noah-MP LSM was developed with the aim of addressing the shortcomings of the original Noah LSM which had a composite layer of surface soil and vegetation over which the surface energy flux was computed Niu et al. (2011), and a bulk layer consisting of snow and soil, which led the model to under-perform in some experiments. Noah MP uses a vegetation canopy layer to separately assess the surface temperature and the canopy, a radiation transfer scheme, a snow model and a scheme for frozen soil, basically enabling the model to overcome previous limitations supporting multiple parametrization options for physical processes, allowing it to be used flexibly and in coupled model setups. Dust modeling with Noah-MP assumes all non-vegetated ground is potentially erodible unless schemes specify otherwise.

CLM The second land surface scheme that we have used is the CLM4 consists of an advanced terrestrial model with improved land cover and vegetation, surface albedo parameters and soil thermodynamics. The hydrology scheme in the model includes an improved Richards equation solution and a revised ground evaporation treatment that accounts for litter and canopy stability (Lawrence et al., 2011). In CLM4, the fraction of bare (erodible) soil in a grid cell is computed explicitly. CLM4 offers a dynamic land model that explicitly links soil moisture, vegetation and texture to dust sources.

In comparison, CLM4 uses a deep soil column with multiple layers to update soil moisture and temperature, while Noah-MP typically uses up to 3–4 soil layers. CLM4's detailed moisture profile makes its surface wetness (and thus dust emission threshold) respond strongly to soil moisture content, whereas Noah-MP's thinner profile emphasises bulk soil moisture behaviour.

https://doi.org/10.5194/egusphere-2026-1900
Preprint. Discussion started: 19 June 2026

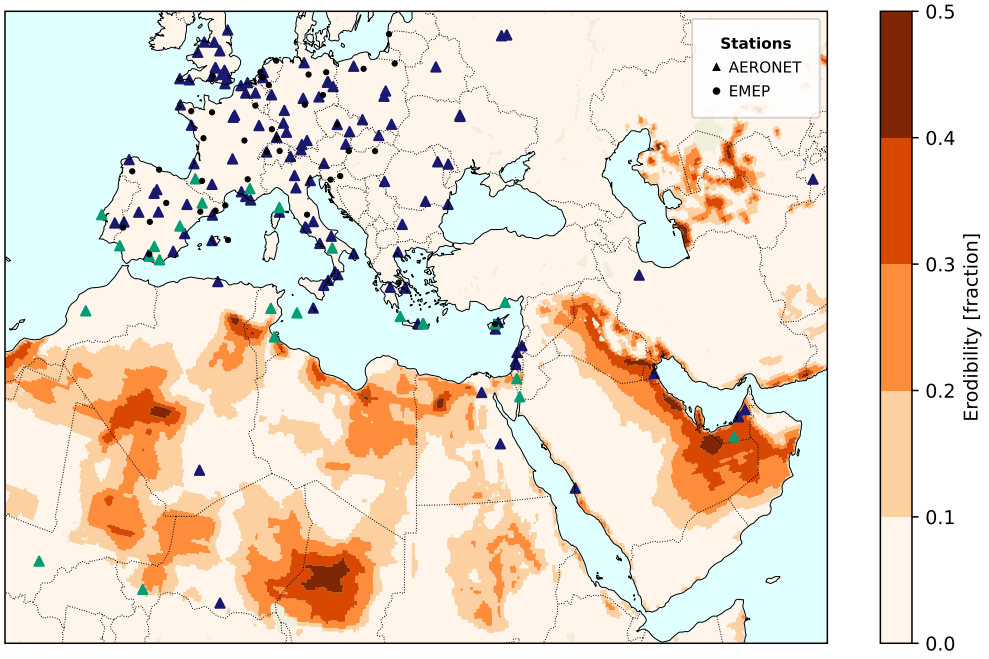

Figure 1. Map of the modelling domain showing all monitoring stations with available measurements. The AERONET network station locations are shown as triangles (green indicates background stations selected for the calculation of statistical metrics; more details on classification in Sec. 4.1.2), and EMEP network stations are shown as black circles. Background shading over land shows the erodible sand fraction from the WRF geogrid dataset, highlighting dust source regions in the model domain.

3 Observation Datasets for Model Evaluation

The WRF-Chem model output is evaluated against observations from the ground-based stations of the AERONET (Sec. 4.1.2) and EMEP (Sec. 3.2) networks, the MIDAS product derived from MODIS satellite retrievals (Sec. 3.3), and surface fiels of the ERA5-Land reanalysis (Sec. 3.4).

3.1 Aerosol Robotic Network (AERONET)

AERONET is a global network, managed by NASA (Holben et al., 1998), operating over 1700 stations, which provides long term measurements of optical parameters of aerosol products. AERONET retrievals can be found for three levels of quality assurance; Level 1.0, 1.5 and 2.0, with level 2.0 being the highest quality-assured with cloud screening. For maximum data coverage across the modelled period and to minimize unscreened or uncalibrated raw measurements, the Level 2.0 time-series was selected for all 146 stations in our domain, (Fig. 1) however for maximum data coverage across the modelled period the dataset was gap-filled using the next highest available quality levels, due to the sparse availability of Level 2.0 data at certain locations (Giles et al., 2019).

https://doi.org/10.5194/egusphere-2026-1900
Preprint. Discussion started: 19 June 2026

To allow consistent comparison between observations from AERONET and modelled AOD, the following computational adjustments were implemented. We tackle the lack of temporal continuity of AERONET measurements by harmonizing observation times through averaging data within a window of ± 30 min of each UTC hour. AOD retrievals from AERONET are not always available directly for the model output short-wave wavelength of 550 nm. The next available wavelength was transformed to equivalent AOD_{550} using the Ångström exponent, following the method described in Kiriakidis et al. (2023). Finally, to limit the comparison to dust-dominated aerosol conditions, the hourly AERONET data was filtered to only include values where AOD observations had values greater than 0.15 and additionally where the 440–870 nm Ångström exponent was lower than 0.75 (Gkikas et al., 2021; Kiriakidis et al., 2023).

AOD_{550} is calculated from the WRF model output as:

$$AOD_{(t,\mathrm{lat,lon})} = \sum_{V=1}^{N_{\mathrm{lev}}} EC55_{(t,\mathrm{lev,lat,long})} \cdot \Delta H_{(t,\mathrm{lev,lat,long})}$$

where H is the model level height (km), ΔH the inter-level thickness, $EC55$ the extinction coefficient at 550 nm (km^{-1}), V the vertical level index up to a total of $\mathrm{N_{lev}}$, t the time, and `lat` and `long` the spatial coordinates.

3.2 EMEP

The European Monitoring and Evaluation Programme(EMEP) is a long-term atmospheric monitoring network established under the UNECE Convention on Long-Range Transboundary Air Pollution (CLRTAP). It is an open-access database that provides high-quality measurements of atmospheric pollutants across Europe. We obtained EMEP data for PM_{10} and $\mathrm{PM}_{2.5}$ from the EBAS database, operated and managed by the Norwegian Institute for Air Research (NILU). EMEP stations provide observations at irregular and often coarse temporal resolution, hence, the hourly WRF output was temporally averaged based on the corresponding EMEP observation window to ensure a consistent comparison.

3.3 MODIS Dust Aerosol (MIDAS)

The ModIs Dust AeroSol (MIDAS) dataset is a global dust optical depth product developed by Gkikas et al. (2021), originally available for the 2003–2017 period. It provides high resolution(0.1×0.1 degrees) daily column-integrated dust optical depth (DOD) at 550 nm globally, from quality-filtered MODIS-Aqua Collection 6.1 (Level 2) AOD retrievals, with DOD-to-AOD ratios provided by the Modern-Era Retrospective analysis for Research and Applications version 2 (MERRA-2) reanalysis.

In order to facilitate a comparative analysis, we extended the dataset to our model simulation period using the same MIDAS derivation methodology. To perform the MIDAS derivation, AOD 550 nm MODerate resolution Imaging Spectroradiometer (MODIS) satellite products were sourced from the L3 MODIS-Aqua Collection 6.1 of NASA's Earth Observing System (EOS) at a resolution of $1° \times 1°$ (Platnick, King, & Hubanks, 2017). The second component of the MIDAS dataset was acquired from MERRA-2 reanalysis, which is a global atmospheric reanalysis dataset produced by NASA's Global Modeling and Assimilation Office (GMAO) (Gelaro et al., 2017). Specifically, the columnar dust extinction AOT and total dust extinction AOT variables at 550 nm were obtained from the `M2T1NXAER` product, version 5.12.4, at a resolution of $0.5° \times 0.625°$ (Global Modeling and

https://doi.org/10.5194/egusphere-2026-1900
Preprint. Discussion started: 19 June 2026

Assimilation Office [GMAO], 2015). MIDAS integrates the MODIS AOD retrievals with the MERRA-2 computed dust fraction from the ratio of atmospheric light extinction from dust (τ_{Dust}) to total atmospheric light extinction (τ_{Total}) from scattering and absorption:

$$\text{MIDAS}^{*} = \text{AOD}_{550}^{\text{MODIS}} \times \left(\frac{\tau_{\text{Dust}}^{\text{MERRA-2}}}{\tau_{\text{Total}}^{\text{MERRA-2}}} \right) \quad (1)$$

MODIS and MERRA-2 products were obtained from the Giovanni data access platform provided by the NASA Goddard Earth Sciences Data and Information Services Center(GES DISC).

3.4 ERA5-Land Reanalysis

ERA5-Land is an enhanced global reanalysis dataset focused on land surface variables, produced by the European Centre for Medium-Range Weather Forecasts (ECMWF) as part of the Copernicus Climate Change Service of the European Commission. The dataset spans the period from 1950 to the present, with a horizontal resolution of 9 km. In ERA-5 soil moisture is analysed for four volumetric soil water layers: (0-7, 7-28, 28-100, 100-289) cm.

In this study, 10 m wind speed and soil moisture fields derived from the six WRF model configurations were evaluated against the corresponding ERA5-Land data. Surface wind speed and soil moisture are controlled by the WRF land surface model and are critical for the emission of dust as they control wind-erodible soil fraction and dust emission via exceeding of the threshold velocity. For soil moisture, we note that there are differences in the definition of soil layer thickness across land surface schemes. The Noah-MP scheme employs four soil layers with thicknesses of 0.1, 0.3, 0.6, and 1.0 m (total depth of 2.0 m), while the CLM4 scheme defines ten layers with thicknesses of 0.018, 0.028, 0.045, 0.075, 0.124, 0.204, 0.336, 0.553, 0.913, and 1.506 m (total depth of 3.8 m).

The comparison with ERA5-Land was conducted using the near-surface soil moisture (layer 1, 0-7 cm). For the WRF simulations, the soil moisture of the uppermost model layer was used, despite differences in layer thickness relative to ERA5-Land. A weighted linear interpolation approach based on layer thickness could be applied to align the vertical representation of soil moisture between datasets; however, we have checked this and found that such an adjustment introduced negligible differences for the near-surface layer. Consequently, only the first model layer was used for this comparison across the different land surface schemes.

4 Results

Model performance in simulating AOD was assessed using AERONET ground-based observations, satellite retrievals, and reanalysis datasets. Furthermore, surface parameters such as wind speed and soil moisture, were evaluated against ERA5-Land dataset.

https://doi.org/10.5194/egusphere-2026-1900
Preprint. Discussion started: 19 June 2026

4.1 Dust Aerosol Optical Depth

As outlined in Sec. 1, dust model simulations exhibit systematic, approximately linear scale biases that are commonly addressed through the application of empirical correction factors. Also our results indicate a persistent bias of dust loading, notably for the GOCART and AFWA dust emission schemes. To mitigate this, we apply empirical scaling factors, already implemented within the respective emission parameterisations, derived from MIDAS dust AOD observations over the simulated domain. The annual mean AOD maps compare grid-cell WRF output with MIDAS values, using bilinear interpolation for collocation (Fig. 2). Scatter plots of these grid-cell AOD values yield the line of best fit between simulated and MIDAS AOD, from which the reciprocal of the slope provides the scale factor used to multiplicatively adjust the simulation dust emissions. The dust emission scale factors (Table 2) are therefore derived from a domain-wide fitting of column dust AOD to MIDAS. The evaluation is based only on the emission-scaled model results. The uncertainties associated with the scale factors are further discussed in Sec. 5. The AERONET and EMEP measurements provide independent evaluation of the AOD temporal variability and near-surface mass concentrations after applying the scale factors.

4.1.1 MIDAS

Figure 2 presents the skill of the model performance for dust aerosol optical depth against the MIDAS dataset, illustrating differences in bias, correlation, and spatial patterns across the various model configurations. The AOD map from MIDAS observations provides the reference distribution used for validation over our domain highlighting the dust dominated regions of the Mediterranean, the Arabian peninsula and large portions of the Sahel region, with AOD values reaching up to 1.5 distinctly observed near the strong emission sources such as the Bodélé depression. When compared against our model simulations, we find substantial differences between the different dust emission schemes and LSM configurations. The GOCART scheme coupled with both the LSMs shows very little differences, generally below 0.2, with MIDAS over the entire domain, exhibiting stronger agreement around the Mediterranean basin compared to AFWA and UoC where differences reach up to 1.5 in some locations. This configuration, however, overestimates dust AOD in certain regions over Sahel, the central and eastern Sahara and this is more pronounced when we move from CLM4 to Noah-MP with GOCART emissions. The AFWA scheme displays similar characteristics to the GOCART mechanism, again with slight overestimations within 0.25 in AOD, in the aforementioned regions. In contrast to Noah-MP, a consistent though subtle underestimation appears over the Arabian Peninsula with the CLM4 configuration. Among the three schemes, UoC exhibits the strongest deviations from MIDAS. Coupled with CLM4, UoC produces moderate regional biases of at least 1.75 for AOD, along with pockets of underestimation over parts of the Middle East. Conversely, the Noah-MP configuration results in extensive and intense positive biases, especially over the Arabian Peninsula, clearly differing from the more consistent and spatially uniform performance of both AFWA and GOCART.

Following the spatial differences, the scatter plots in the bottom panel of Fig. 2 summarise how each configuration performs against MIDAS at all collocated model grid-points. The applied empirical scaling factors align the modelled AOD with the observed magnitude, ensuring a consistent basis for comparison across schemes. The stronger clustering along the 1:1 line for AFWA and GOCART reflects their better precision, which is also supported by their higher correlation coefficients ($R^2 =$

https://doi.org/10.5194/egusphere-2026-1900
Preprint. Discussion started: 19 June 2026

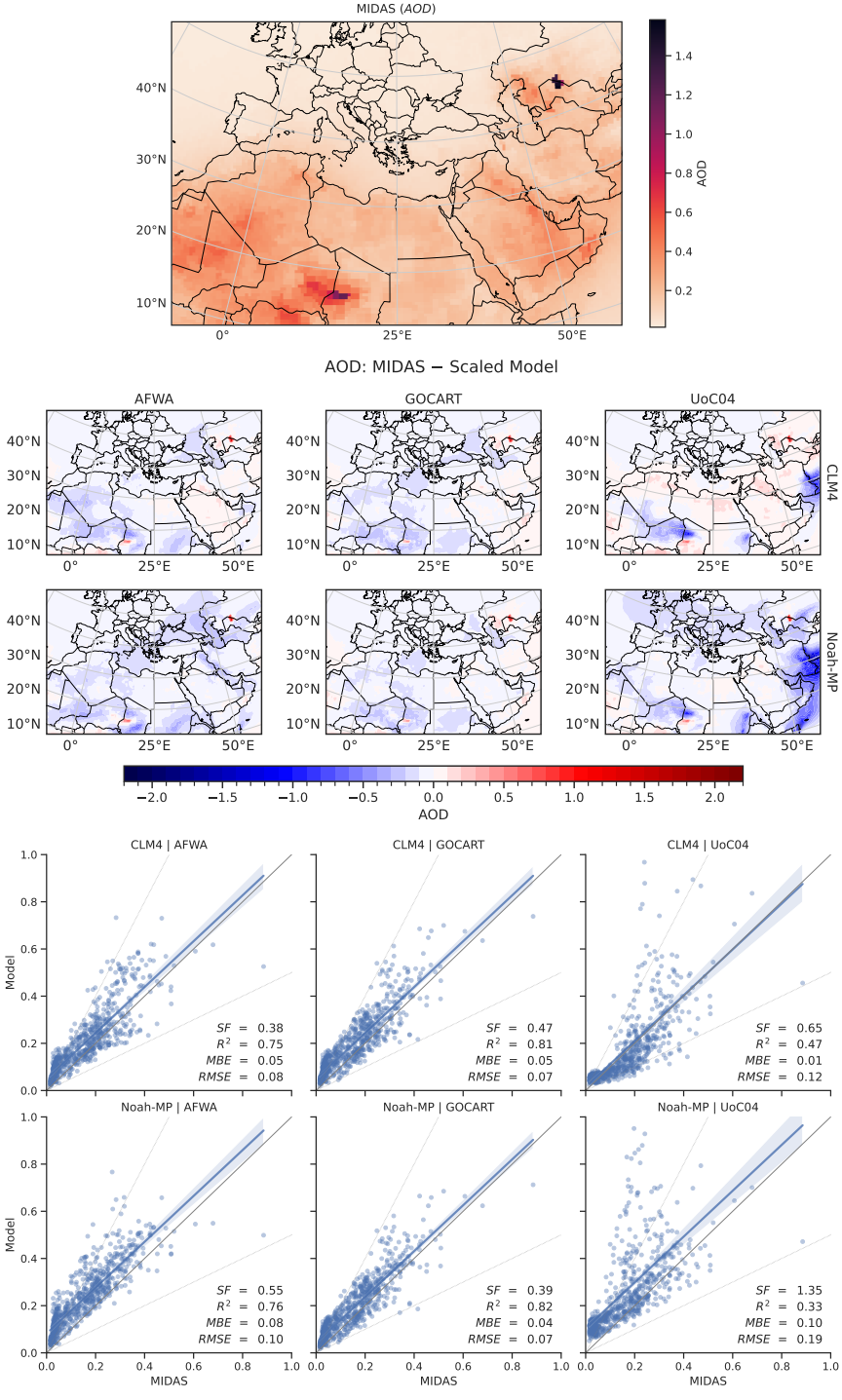

Figure 2. Annual average MIDAS dust AOD (top), ensemble difference between MIDAS and modelled dust AOD (middle), and equivalent scatter plots of model dust AOD against MIDAS with lines of best fit and statistical metrics (bottom).

https://doi.org/10.5194/egusphere-2026-1900
Preprint. Discussion started: 19 June 2026

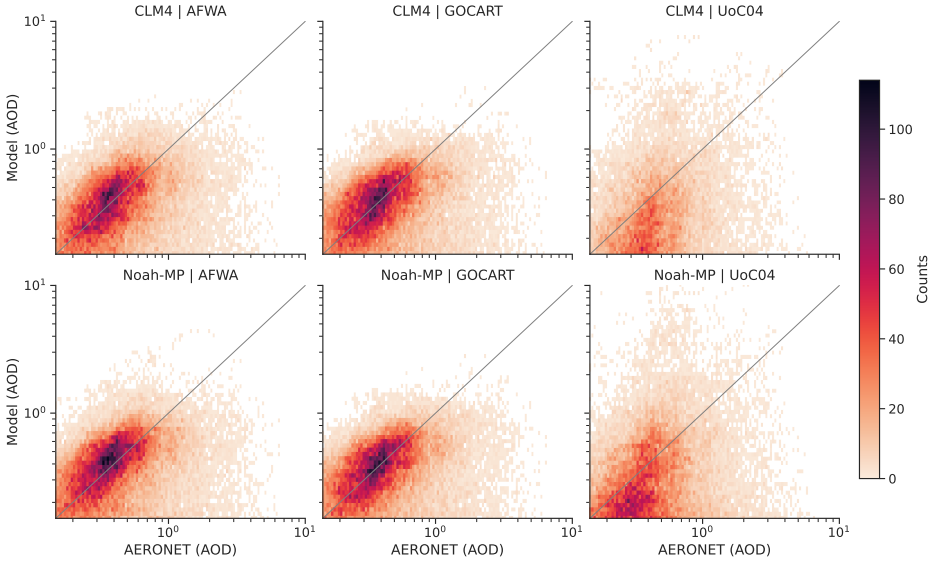

Figure 3. Frequency distributions of modelled versus observed dust AOD at all AERONET station locations in the modelled domain for the different dust emissions and LSM combinations.

$0.75-0.82$) relative to the UoC configurations ($R^2 = 0.33, 0.47$). UoC shows a much wider spread, in particular when coupled with Noah-MP, with correlation as low as $R^2 = 0.33$, consistent with the large positive biases previously identified.

4.1.2 AERONET

To further assess the model skill in reproducing observed dust aerosol loading, simulated AOD values were additionally compared against hourly AERONET observations from all available ground stations and over the full temporal coverage of the measurements (Fig. 3). The scatter density plots reveal systematic differences in model behaviour, highlighting variations in bias and spread between the configurations. Among the three dust emission schemes, GOCART (middle column) demonstrates the strongest correspondence with AERONET observations (evaluation metrics are reported in Table 1). This indicates that the GOCART configuration reproduces the observed AOD magnitudes more realistically and captures a larger portion of the variability across sites and time periods, with a mean absolute error of 0.33, closely followed by AFWA, which also performs reasonably well, with a similar mean normalized error ($\sim 62\%$) and absolute error (0.33) for moderate AOD values. The UoC scheme exhibits systematically larger error magnitudes, with NME values that are approximately 20–30% higher than those of the other schemes, particularly when coupled with CLM4, implying this parametrization under-represents dust emissions or fails to sustain sufficient aerosol loading in the atmosphere, regardless of the land surface model used. This represents a notable limitation, in particular since in Fig. 2 when coupled to the Noah-MP LSM, UoC exhibits a tendency towards systematic overestimation in the whole domain across the AOD range, and notably at the very low AOD values close to zero, evident from comparing the line of best fit to the 1:1 line and lack of points at the origin. Overall, comparison with AERONET indicates

https://doi.org/10.5194/egusphere-2026-1900
Preprint. Discussion started: 19 June 2026

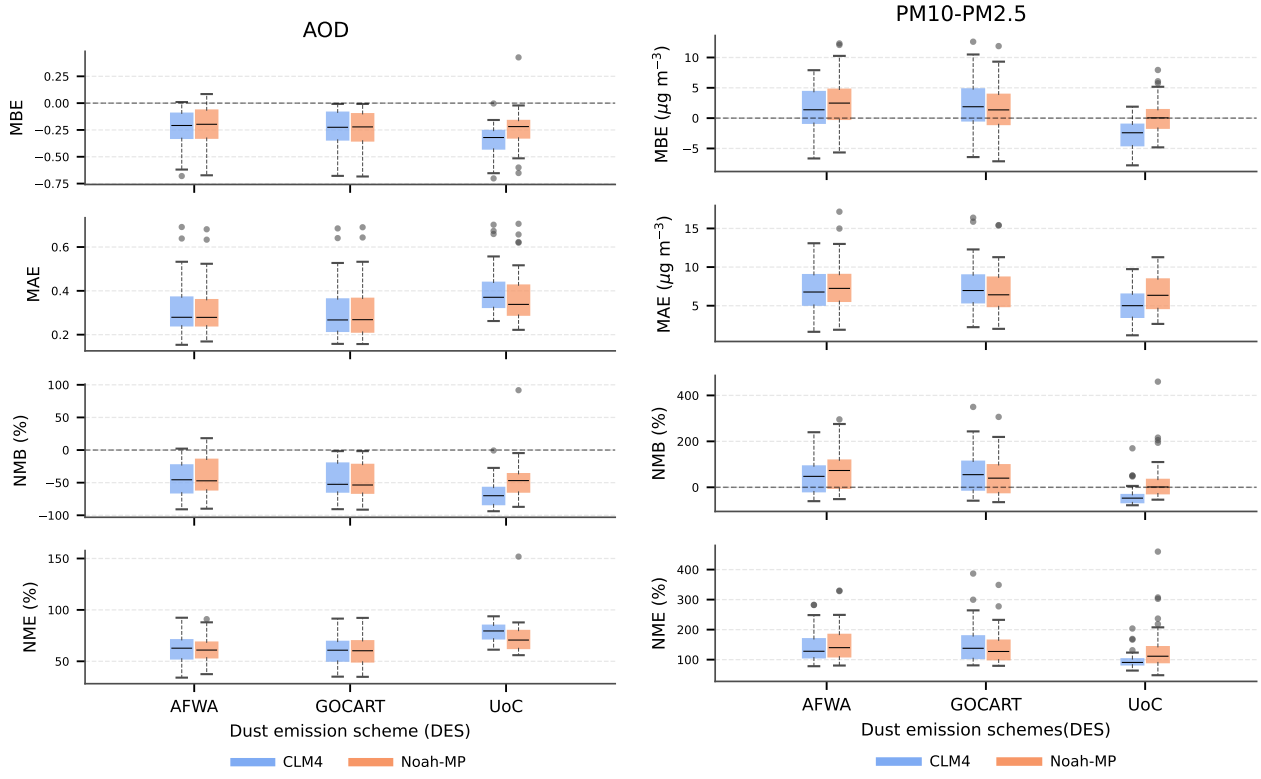

Figure 4. Model ensemble statistical metrics for dust AOD at low-built-up areas AERONET stations (left) and coarse PM ($PM_{10} - PM_{2.5}$) at EMEP stations (right), top-to-bottom: Mean Bias Error (MBE), Mean Absolute Error (MAE), Percentage Normalised Mean Bias (NMB) and Normalised Mean Error (NME). The boxes encompass the inter-quartile range (IQR: 25-75% of values) and whiskers include the range [25%-1.5×IQR, 75%+1.5×IQR], medians are shown as black lines within the boxes, and outliers are shown as grey dots. Target values are shown as black dashed lines.

distinct variations in simulated AOD distributions between the two land surface model configurations. Noah-MP generally produces higher AOD values (with differences generally in the range 0.1–0.3, and up to 0.5 at higher AOD) and a broader dynamic range compared to CLM4, particularly for the AFWA emission scheme where the difference between the two LSMs is most evident. For the UoC scheme, both LSMs result in reduced accuracy and consistent low precision in AOD relative to observations, with the Noah-MP simulations exhibiting a slightly wider range of values. Overall, the influence of the land surface model on simulated AOD appears to be very scheme-dependent, with notable sensitivity for AFWA and consistent underperformance for UoC. The above analysis also aligns with the findings from the satellite derived MIDAS evaluation, strongly supporting the robustness of GOCART emission scheme.

In order to quantify the diagnostic skill of the model-simulated AOD with respect to the observations from AERONET, we apply a set of widely adopted statistical metrics, namely Mean Bias Error (MBE), Mean Absolute Error (MAE), Percentage

https://doi.org/10.5194/egusphere-2026-1900
Preprint. Discussion started: 19 June 2026

Normalised Mean Bias (NMB) and Normalised Mean Error (NME), as defined in Appendix B. For the calculation of statistical metrics, we apply a selection based on the ESA WorldCover built-up layer map to avoid stations affected by local anthropogenic dust sources in built-up areas. All stations in our modelled domain were ranked according to the fraction of WorldCover built-up area within a 5 km radius around each station site, and the 40% least built-up sites were retained. This filtering ensures that the retained stations are subject to limited influence by local anthropogenic activity and more representative of naturally emitted and transported dust. Figure 4 summarizes the comparative performance of the different combinations for each statistical metric. The plots show that AFWA and GOCART exhibit stronger agreement with the observations with MBE of -0.25 averaged over all sites, whereas UoC performs substantially weaker with MBE ranging from approximately -0.35 to -0.25. Although, GOCART and AFWA achieve broadly comparable skill across all the metrics, with the interquartile ranges and median values remaining stable between the two LSMs, minute LSM dependent differences appear particularly in the NMB in terms of the median values. For AFWA emissions, the Noah-MP LSM tends to produce higher AOD values and a broader spread compared to CLM4. The mean bias errors highlight differences between dust emission schemes, with the median values ranging from -0.4 to -0.2. UoC stands out with larger negative biases, wider MAE distributions ($\sim 0.39 - 0.41$) and elevated medians including high magnitude outliers which are evident throughout all the metrics, reflecting greater spread and reduced agreement across the observation network. The difference between the two LSMs is also pronounced in the case of UoC, with CLM4 consistently showing poor performance with average NME up to 78.47%, underlining the strong sensitivity of dust emissions to the land surface model used. In addition to these biases, the MAE=0.33 and NME=61% values indicate that GOCART achieves the smallest absolute and fractional deviations across stations, whereas AFWA exhibits higher error magnitudes despite its comparable mean bias. A summary of the key metrics is provided in Table 1, and the complete set of individual station statistics is included in the Appendix for reference.

Table 1. Summary of evaluation metrics for AOD-AERONET and PM_{10}–$PM_{2.5}$ and EMEP.

Dust Emissions	LSM	AERONET			EMEP		
		MBE	MAE	NME (%)	MBE ($\mu g\,m^{-3}$)	MAE ($\mu g\,m^{-3}$)	NME (%)
GOCART	CLM4	−0.25	0.33	61.23	1.99	7.57	151.41
	Noah-MP	−0.25	0.33	61.28	1.28	7.13	140.99
AFWA	CLM4	−0.24	0.33	62.71	1.36	7.15	141.26
	Noah-MP	−0.22	0.33	61.96	2.40	7.67	153.04
UoC	CLM4	−0.35	0.41	78.47	−2.79	5.22	99.46
	Noah-MP	−0.25	0.39	74.00	0.27	6.55	136.64

4.2 Surface Emission Drivers

To evaluate the surface variables governing dust emission, we compare modelled soil moisture and wind speed with the ERA5-Land reanalysis. This allows us to identify biases in the surface forcing fields that influence the simulated dust fluxes. Figure 5 (top left) illustrates the annual mean soil moisture in the top layer from ERA5-Land, highlighting the strong north-south

https://doi.org/10.5194/egusphere-2026-1900
Preprint. Discussion started: 19 June 2026

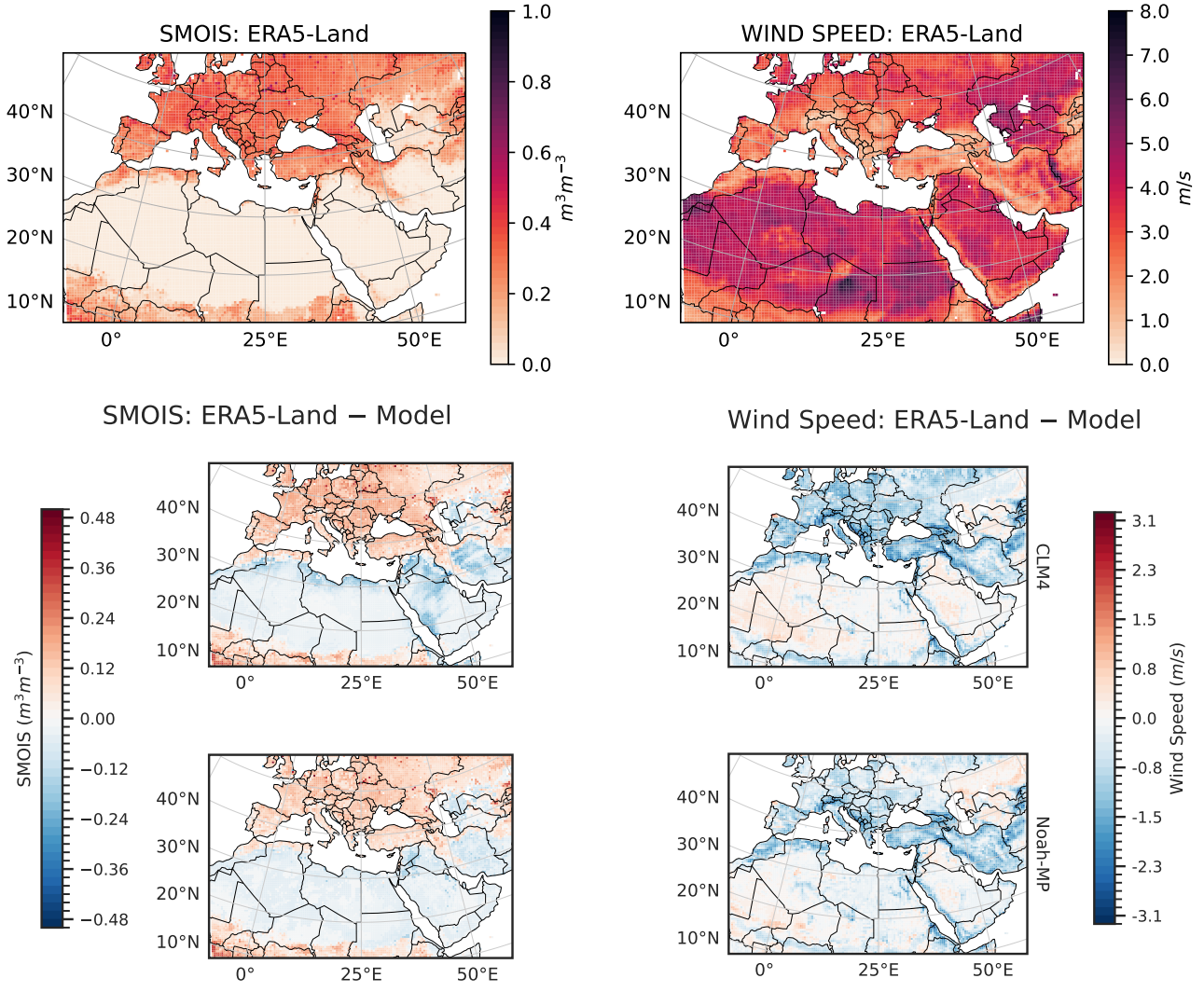

Figure 5. ERA5-land reanalysis annual mean surface soil moisture -SMOIS (top left) and wind speed at 10 m (top right), and spatial differences with WRF-Chem simulations with CLM4 (middle row) and Noah-MP (bottom row) using GOCART emissions.

contrast, with typically drier and arid areas of the Sahel and Arabian Desert as compared to Europe and East Asia. A gradient is also visible in the annual mean 10 m wind speed from ERA5-Land reanalysis (top right), which exhibits enhanced near-surface winds across the relatively flat high-erodibility plains in the Sahel, Arabian Peninsula, and parts of Central Asia.

To examine the model performance we analyse the differences of surface drivers between ERA5-Land and the WRF-Chem LSM simulations. In Fig. 5 we present results only for the GOCART configuration as the behaviour of these surface parameters is largely independent of the choice of dust emissions, and this was confirmed by the highly consistent spatial patterns for all combinations of dust-emission schemes. The full set of results for all ensemble members is presented in the Appendix (Figs. A1

https://doi.org/10.5194/egusphere-2026-1900
Preprint. Discussion started: 19 June 2026

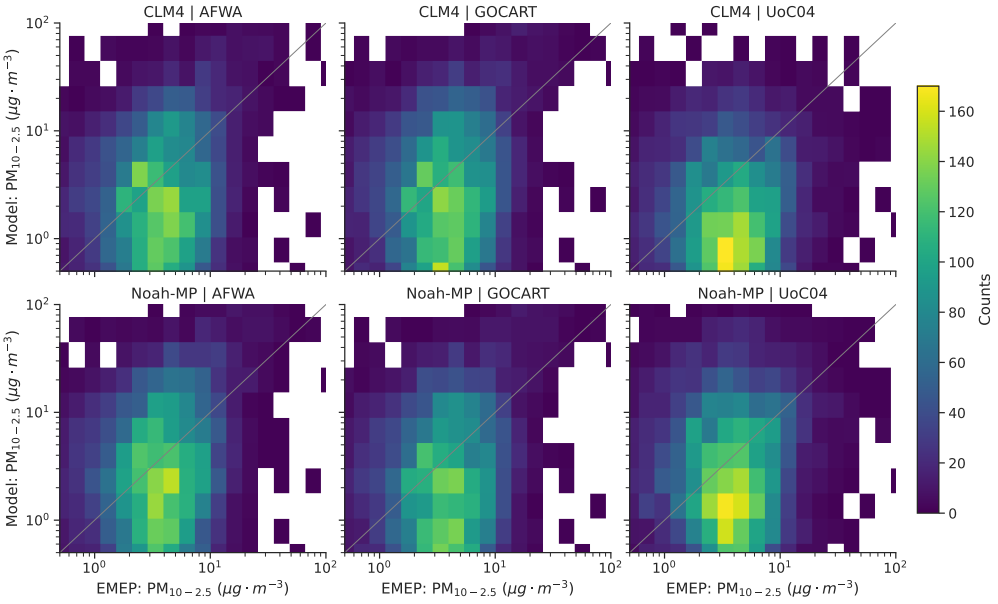

Figure 6. Scatter-density of modelled versus observed daily average $\mathrm{PM}_{10-2.5}$ at selected EMEP stations within the model domain for the AFWA, GOCART and UoC dust emission schemes coupled with CLM4 and Noah-MP.

and A2). Throughout the domain, CLM4 yields positive biases for soil moisture, especially in continental Europe, indicating that CLM4 simulates systematically drier near-surface layers compared to ERA5-Land, with some localised wet biases over the Arabian Peninsula and parts of the Middle East. Wind speeds are systematically overestimated across North Africa, the Southern Europe, and Central Asia by up to 1–3ms^{-1}, with some regional underestimations of up to 2ms^{-1}. Regarding soil moisture, Noah-MP similarly shows improved agreement across most regions, although it still underestimates moisture over Europe and parts of Asia. Noah-MP also exhibits smaller and more spatially uniform deviations for wind-speed, with generally weaker overestimation (negative differences) over Central and Southern Europe and only limited areas of underestimation (positive differences) around the Sahel and the Arabian peninsula. Throughout the domain we note that the comparison with ERA5-Land shows larger deviations in coastal regions, as reflected in the biases evident in our results maps. This behaviour is further outlined in Sect.5.

4.3 Coarse Particulate Matter Concentrations

We evaluated our model performance for surface coarse particulate matter ($\mathrm{PM}_{10} - \mathrm{PM}_{2.5}$) concentrations away from anthropogenic PM sources, which is a proxy for aeolian dust in our domain (Sciare et al., 2003; Pikridas et al., 2018), against observations from the EMEP network.

Figure 6 presents 2-D density scatter plots of the daily average modelled vs observed coarse PM concentration for all ensemble members. We note that EMEP observations are restricted to Europe, while the model covers the broader EMME region,

https://doi.org/10.5194/egusphere-2026-1900
Preprint. Discussion started: 19 June 2026

so the results presented here are limited in representativeness to the European subset of our domain. EMEP measurements are reported at multiple temporal resolutions; model output was aggregated to matching hourly or daily averages prior to comparison. To minimise discretisation effects and preserve temporal fidelity, only stations reporting the full decimal range were retained. In all cases, the modelled versus observed distributions show some precision, but with some systematic accuracy deviations, particularly across low to moderate concentrations. With UoC dust emissions, we obtain a more compact distribution, particularly when coupled with the Noah-MP LSM, with prominent underestimation for CLM4. Unlike for the MIDAS and AERONET AOD evaluations, UoC is found to perform better in this metric which indicates that it is more capable of capturing the emissions dynamics and mass loading distribution for coarse dust particulates. The comparison with EMEP coarse PM is subject to several limitations (see Sect. 5), including mixed aerosol contributions, incomplete representation of aerosol processes in the model, and rounding artefacts in the observational dataset.

Further analysis of this comparison through statistical metrics using all available EMEP stations across the domain, is presented in Fig. 4. We find that the median of the MBE values remains close to zero overall, while MAE values range from 5–15 μg m^{-3}. The distributions for AFWA and GOCART metrics exhibit a wider spread with small variations when subjected to different LSMs. UoC in this case consistently shows the best performance, specially when coupled to CLM4. A consolidated summary of all statistical metrics is provided in Table 1, while the complete results for individual stations can be found in the Appendix.

5 Discussion

The results presented above reveal several systematic differences between emission schemes and land surface model configurations and the irregularities are interpreted in this section. Evaluated against the MIDAS dataset, GOCART and AFWA produce closer agreement with correlation coefficient 0.81–0.82, with slight positive biases as already highlighted in section 3.3. This good agreement relative to UoC in column AOD may be attributed to how each scheme represents dust emission. GOCART assumes that dust is emitted mainly from topographic depressions where fine sediments accumulate (Ginoux et al., 2001), which helps capture the main large spatial-scale dust source regions and the lofting and long-range transport of fine dust particles. The stronger spatial variability in the UoC scheme may be attributed to its representation of saltation and sandblasting. In this scheme, dust emission depends directly on soil aggregate size and soil moisture (Shao, 2001; Marticorena and Bergametti, 1995). Since soil moisture increases the threshold friction velocity (Kok et al., 2012), small changes in surface conditions can strongly affect the emitted dust flux. This sensitivity could explain the larger regional differences seen in UoC. A consistent pattern emerges from the comparison with AERONET observations, which similarly indicates improved performance of the GOCART and AFWA schemes relative to UoC, particularly in terms of reproducing observed AOD magnitudes and variability. The bias maps presented in Fig. 2 are constructed by subtracting grid-cell WRF values from MIDAS values, with bilinear interpolation used to regrid the datasets onto a common grid. Unlike satellite retrievals, model simulations provide continuous temporal coverage without gaps. It is worth noting that in Fig. 2 a consistent AOD peak is present over the Aralkum Desert near the Caspian Sea in MIDAS, which is reflecting strong dust and salt aerosol emissions from the bare Aral Sea basin. Although

https://doi.org/10.5194/egusphere-2026-1900
Preprint. Discussion started: 19 June 2026

this region constitutes a significant dust source with long-range transport potential (Indoitu et al., 2015), the reliability of these elevated values of DOD (>1) needs to be interpreted with caution (Gkikas et al., 2022). WRF-Chem does not reproduce this feature, likely due to insufficient representation of Aralkum in the land-use and erodibility inputs and the spatial resolution smoothing effect of the model preprocessor on a localized emission source (Banks et al., 2022; Xi et al., 2025).

The evaluation against EMEP stations measurements (Sec. 3.2) suggests comparatively better skill of the UoC scheme in simulating near-surface coarse PM. This can be attributed to UoC's explicit parametrization of saltation bombardment and aggregate disintegration (see Sec. 2.1), which produces a particle size distribution featuring a more realistic coarse fraction that then better represents surface concentrations at distant receptors in Europe after long-range transport. This could also be in part due to EMEP stations being further away from the dominant fine (clay and silt) dust sources and only sampling the surface boundary layer, which is dominated by the sedimentation of coarser (sand and gravel) dust particles, along with stronger influence from local emissions and other primary aerosols like sea salt in coastal areas. The coarse PM fraction ($\mathrm{PM}_{10} - \mathrm{PM}_{2.5}$) includes in addition to dust, sea-salt and other anthropogenic primary aerosols. Also, our simulations do not account for secondary anthropogenic and biogenic aerosols. Thus, uncertainties in representation of natural sea-salt emissions, transport and removal processes, along with the fraction of dust and sea salt emitted in each bin in the sectional aerosol model affects the comparison with EMEP coarse PM. We acknowledge these limitations and do not examine them further as they lie beyond the scope of this work. Further, it should be noted that for a number of EMEP stations there exist numerical rounding/precision artefacts in the reported values that inadvertently introduce discontinuities in the observation distribution, so the coarse PM comparisons should in any case be interpreted with caution.

The evaluation of surface meteorological fields with ERA5 land presented in Sec. 3.4 highlights larger deviations in coastal regions. This arises from the sharp land–sea contrasts in surface roughness and radiative forcing, which create strong gradients that are difficult to resolve by the model (Gualtieri, 2021; Bessonova et al., 2025), and additionally the challenge to reconcile between the different spatial resolutions of each pre-processed input and evaluation dataset.

We note that in our modelling framework, the initial and boundary conditions (and nudging) for all simulations were produced using the NCEP FNL dataset. While different meteorological reanalysis products may introduce some variations in model initialisation and subsequent dynamic evolution (Wu et al., 2025; Wang et al., 2024), sensitivity assessments using alternative datasets such as ERA5 are not examined here and remain a possible direction for future studies.

Finally, we provide reference empirical dust emission scale factors (Table 2) for all combinations of emission mechanisms and LSMs, that are applicable to be used in WRF-Chem model simulations. The scale factors presented in Table 2 are in principle applicable to all WRF-Chem simulations, with equivalent dust-emission-LSM parameterisation configurations, encompassing aeolian dust emissions from sources in the dust belt. To test the resolution dependence, we conducted sensitivity tests for the three dust emission schemes with CLM4 at higher horizontal resolution (10×10 km grid spacing) for the first 24 days of the simulated year and compared over the same period with the simulations at 50 km resolution that the scale factors reported in Table 2 were derived from. The results indicate that the scaling factors reported here are effectively resolution-independent for GOCART and show only marginal variation for AFWA ($\sim 6\%$) and are therefore applicable to model grid spacings on the order of 10–100 km. The UoC emission scheme exhibits a marked resolution-dependent behaviour, as we ob-

https://doi.org/10.5194/egusphere-2026-1900
Preprint. Discussion started: 19 June 2026

Table 2. Empirical scale factors for dust emissions – land surface model WRF-Chem model configurations.

Dust Emissions	Land Surface Model	Scale Factor
GOCART	Noah-MP	0.39
	CLM4	0.47
AFWA	Noah-MP	0.55
	CLM4	0.38
UoC	Noah-MP	1.35
	CLM4	0.65

tain a difference of 35% in the resulting scale factor. The uncertainties associated with resolution effects and their underlying causes are discussed in more detail in the Appendix.

6 Conclusions

We present a full-year exhaustive study of the performance of the WRF-Chem model representation of mineral dust emission and transport in the atmosphere over and around the global dust belt. Emissions of aeolian dust continues to be a dominant source of uncertainty in regional and global models, with dependence on modelled land surface properties, meteorological drivers, and parametrisations to capture complex multi-scale processes. In spite of the widespread use of WRF-Chem in modelling the atmospheric dust cycle, long-term multi-configuration evaluations are lacking in the literature, particularly encompassing the whole of the climatologically active dust belt, comprising the major global sources of dust aerosol, extending from North Africa across the Middle East to Central and East Asia. Accurate characterisation of dust aerosol loading is critical for understanding radiative effects, and refining weather and climate applications.

Our WRF-Chem model experiment cohort comprises six members, formed by the pairing of three dust emission schemes (GOCART, AFWA and UoC) and two state-of-the-art land surface models (CLM4 and Noah-MP). Model simulations were run throughout a full calendar year. Our model domain encompasses all natural dust emission sources within the dust belt, as well as the adjacent receptor regions. The results of our numerical experiments are evaluated against the MODIS obtained MIDAS dataset of Dust Aerosol Optical Depth (AOD) at 550 nm, and MERRA2 reanalysis. The analysis reveals that GOCART emissions achieve the strongest agreement with MIDAS, with $R^2 \gtrsim 0.8$, with particularly good agreement over Europe and the Middle East, and with minor differences near the dust source regions of the Sahel. This is similar for AFWA dust emissions, although in this case the choice of LSM introduces noticeable differences, most evident near the Arabian desert. UoC exhibits poor performance with very low R^2 correlations, down to 0.47 for CLM4 and 0.33 for Noah-MP.

The additional validation with ground based AOD measurements from AERONET reinforces the MIDAS-based conclusions, identifying GOCART as nearest to the observed values, closely followed by AFWA, and UoC consistently underperforming with distinct underestimation of lower AOD values for both LSMs. The analysis of statistical metrics computed for the selected

https://doi.org/10.5194/egusphere-2026-1900
Preprint. Discussion started: 19 June 2026

background AERONET stations shows UoC performing markedly weaker with 18-24% higher MAE values, (Fig. 4, Table 1), further supporting these findings.

We compared key surface dust emission LSM parameters from our simulations against the ERA5-Land reanalysis. The results indicated that Noah-MP captures the large-scale patterns of soil moisture and near-surface winds more consistently, whereas CLM4 introduces pronounced regional discrepancies, in particular across North Africa. Given that surface wind and soil moisture directly control threshold friction velocities and dust erosion fluxes, our results imply that Noah-MP provides a more reliable surface boundary condition for dust-modelling applications, with pronounced differences arising from the choice of LSM in WRF-Chem model simulations. The systematic overestimation of wind speeds across North Africa by 1-3 m/s serves as a primary driver for the dust loading biases observed in the GOCART and AFWA schemes. While Noah-MP provides a more consistent representation of large-scale soil moisture and near-surface winds, CLM4 introduces regional discrepancies (simulating systematically higher moisture in the surface layer over the dust emission regions), which impacts the dust mobilization potential. These assessments indicate the the model performance is strongly dependent on the choice of dust emission schemes, with land-surface models contributing additional variability by affecting the surface conditions that regulate emission potential.

Furthermore, we find that WRF-Chem coupled with UoC reproduces coarse PM reasonably well over Europe at EMEP network stations, while AFWA and GOCART show a larger spread. Nevertheless, these findings must be interpreted in context of known limitations in the EMEP dataset and the simplified parametrisation of coarse aerosol species within the model.

Based on the year-long evaluation over the dust belt domain, the GOCART dust scheme with Noah-MP LSM and a scale factor 0.39 yielded the strongest agreement with MIDAS dust optical depth and AERONET AOD, making it applicable for column dust loading, radiative forcing, or long-range transport applications. AFWA coupled with Noah-MP and a scale factor 0.55 is a close alternative with comparable performance. For surface coarse mode particulate matter $(\mathrm{PM}_{10} - \mathrm{PM}_{2.5})$ at European EMEP stations, UoC with CLM4 (and a scale factor 0.65) shows the closest agreement among the tested configurations, likely owing to its more realistic coarse dust emission fraction representation. Finally, UoC with Noah-MP and a scale factor of 1.35 may be a suitable alternative when the coarse dust consistency of surface concentrations is prioritised. Sensitivity experiments further indicate that the scaling factors derived for GOCART and AFWA are largely independent of horizontal resolution (see Sec.5) and can therefore be applied to higher resolution simulations, thereby extending their applicability. Conversely, the UoC scheme exhibits a marked dependence on model resolution, and any scaling of emissions should therefore be applied carefully. These conclusions are supported by the statistical evaluation of model skill (metrics in Table 1 and Figs. 3-6, scale factors presented in Table 2) and the resolution-dependence of the coefficient of variation presented in Appendix Fig. A3).

Our study uniquely focuses on capturing a broad spatial domain that is pertinent for aeolian dust simulations with WRF-Chem model, over a representative temporal period of a full calendar year. Rather than focusing on seasonal subsets or individual dust events, the analysis is intentionally conducted over the full annual cycle to provide a general assessment of the model's ability to represent dust behaviour under a wide range of meteorological conditions. Our results lead towards our ultimate objective of understanding the global aeolian dust cycle, by constraining parametric uncertainties and improving the WRF-Chem model capability for operational and climate-scale dust prediction.

https://doi.org/10.5194/egusphere-2026-1900
Preprint. Discussion started: 19 June 2026

Code and data availability. The WRF Model is publicly available as open-source code and can be used without restriction. The WRF-Chem model source code v4.7.1, configuration namelists, and the data used in the model evaluation figures are available in the Zenodo repository at https://doi.org/10.5281/zenodo.19498593 (Deb et al., 2026). The Noah-MP model code is available at Cenlin_He et al. (2023). The meteorological initial and boundary conditions used in this study were obtained from the NCEP FNL dataset, which is available from the National Centers for Environmental Prediction (NCEP) at https://doi.org/10.5065/D6M043C6. The AERONET data can be found on the AERONET website at https://aeronet.gsfc.nasa.gov/cgi-bin/webtool_inv_v3. EMEP data is available at https://ebas-data.nilu.no/.

https://doi.org/10.5194/egusphere-2026-1900
Preprint. Discussion started: 19 June 2026

Appendix A: Supplementary Additional Information

The comparison of WRF-Chem to the ERA5-Land reanalysis reference of 10 m wind speed and surface soil moisture for all ensemble members are presented in Appendix Figs A1 and A2 respectively. Statistical metrics for AERONET and EMEP stations are presented in Appendix Tables A1 and A2 respectively.

The uncertainties associated with empirical scaling factors of simulated aerosol optical depth (AOD) and coarse PM and their dependence on horizontal model resolution are presented here. In addition to the main analysis, which focuses on the horizontal resolution of 50 km, sensitivity tests using the three dust emission schemes with CLM was conducted at 10 km horizontal resolution, to assess the resolution effects on simulated dust aerosol loading and the resulting scaling factors over a 24-day period. Figure A3 shows the spatial distribution of the coefficient of variation (CV=σ/μ, where σ and μ denote the temporal standard deviation and mean of the local difference between two simulations) of simulated AOD between 50 and 10 km in the model domain. The resulting values (Fig. A3) map the relative variability between the simulations in percentage. The coefficient of variation analysis indicates that the response of simulated dust AOD to model resolution varies spatially for the dust emission schemes. The spatial distribution of the coefficient of variation for GOCART and AFWA shows broadly consistent AOD magnitudes between the two resolutions. Even though over the entire domain the scale factors do not vary markedly, Fig. A3 reveals some localised differences (up to 80%) in the northern part of our domain. This is due to local missing sources, and is over northern regions where dust loadings are in any case lower than in closer proximity to the dust belt. In the case of UoC, moderate CV values (generally 20–30%) prevail over large parts of north Africa and the Mediterranean, indicating differences in AOD magnitudes between the two resolutions in these regions along with substantially higher CV values persisting over the Middle East, the Arabian Peninsula, and parts of Southwest and Central Asia, with local maxima exceeding 60—80%. These regions are characterised by strong dust emission sources, where finer-scale meteorological processes play an important role.

We note that, whereas the 50 km simulations were evaluated over a full annual cycle using multiple model configurations, the 10 km sensitivity simulations were restricted to a 24-day period and conducted with a single land surface model for all three dust emission schemes, due to the increased computational demands. Consequently, the resolution-related differences and scaling factors inferred from the 10 km experiments may not fully capture long-term variability or configuration-dependent effects. These results should therefore be interpreted as indicative of resolution sensitivity rather than as definitive conclusions.

https://doi.org/10.5194/egusphere-2026-1900
Preprint. Discussion started: 19 June 2026

Appendix B: Evaluation Statistical Metrics

Mean Bias (MBE):

$$MBE = \frac{1}{N}\sum_{i=1}^{N}(x_{\text{mod},i} - x_{\text{obs},i}) \tag{A.1}$$

Mean Bias Error (MAE):

$$MAE = \frac{1}{N}\sum_{i=1}^{N}|x_{\text{mod},i} - x_{\text{obs},i}| \tag{A.2}$$

Normalized Mean Bias (NMB):

$$NMB = \frac{\sum_{i=1}^{N}(x_{\text{mod},i} - x_{\text{obs},i})}{\sum_{i=1}^{N} x_{\text{obs},i}} * 100 \tag{A.3}$$

Normalised Mean Bias Error (NME):

$$NME = \frac{\sum_{i=1}^{N}|x_{\text{mod},i} - x_{\text{obs},i}|}{\sum_{i=1}^{N} x_{\text{obs},i}} \tag{A.4}$$

Coefficient of Variation (CV):

$$CV = \frac{\sigma}{\mu} \tag{A.5}$$

https://doi.org/10.5194/egusphere-2026-1900
Preprint. Discussion started: 19 June 2026

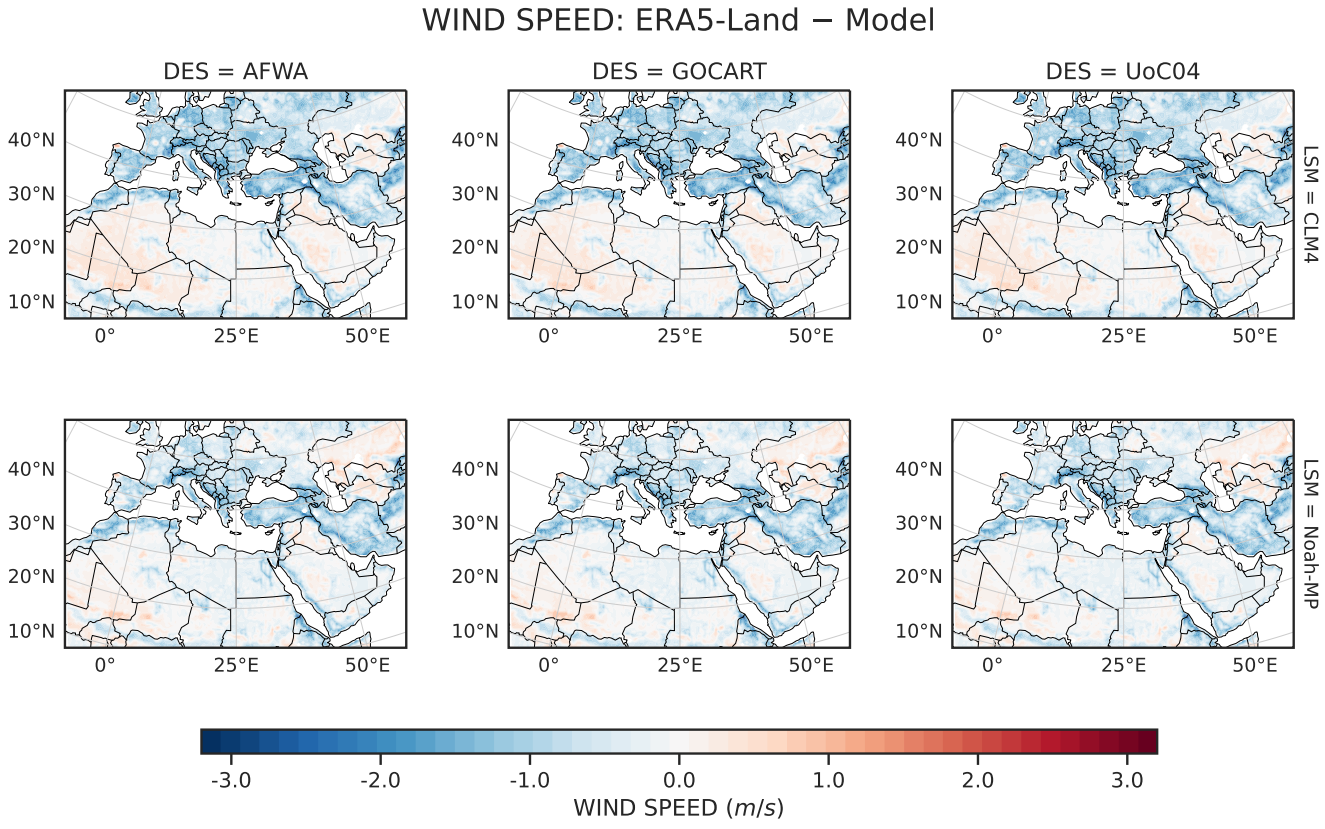

Figure A1. Annual mean wind speed at 10 m differences to ERA5-land reanalysis for the ensemble WRF-Chem simulations.

https://doi.org/10.5194/egusphere-2026-1900
Preprint. Discussion started: 19 June 2026

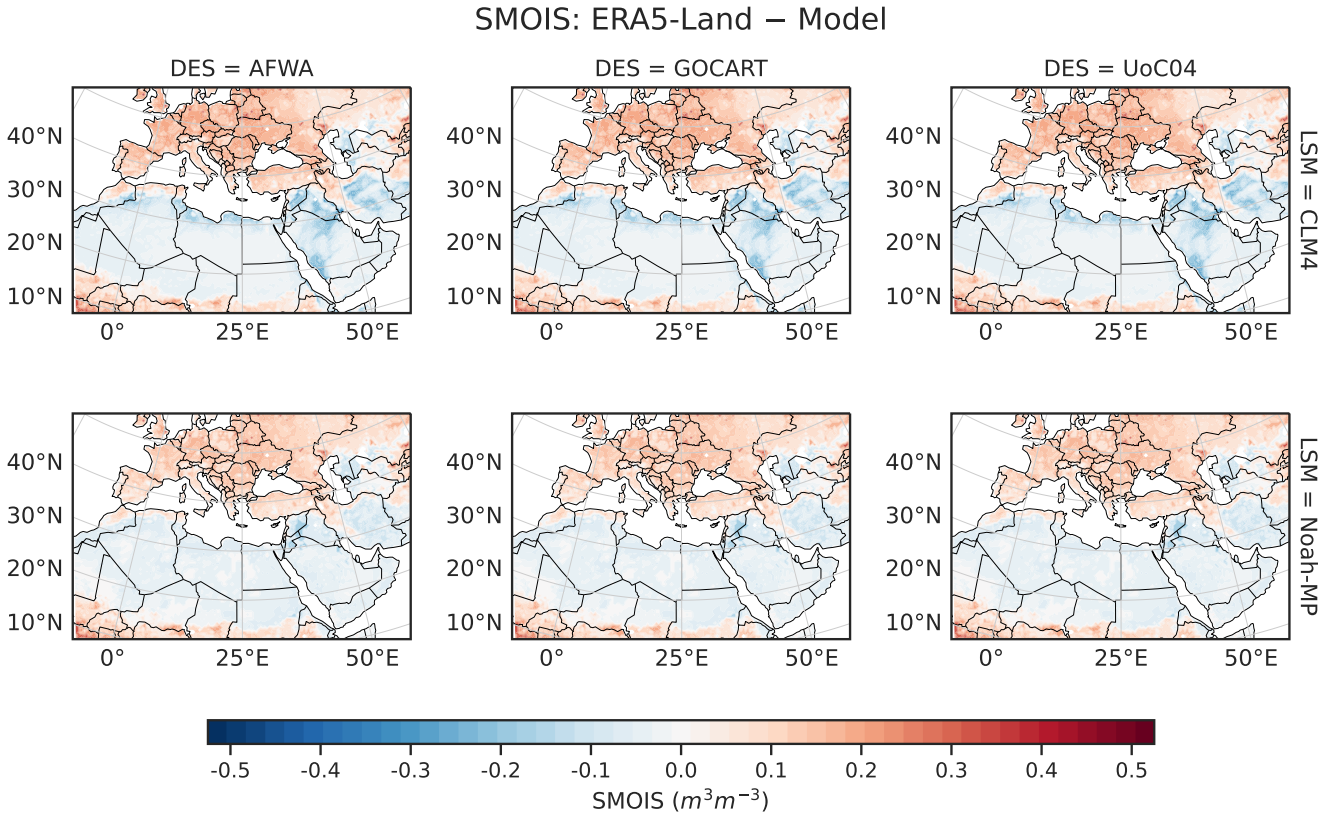

Figure A2. Annual mean soil moisture (SMOIS) differences in $\mathrm{m^3 m^{-3}}$ to ERA5-land reanalysis for the ensemble WRF-Chem simulations.

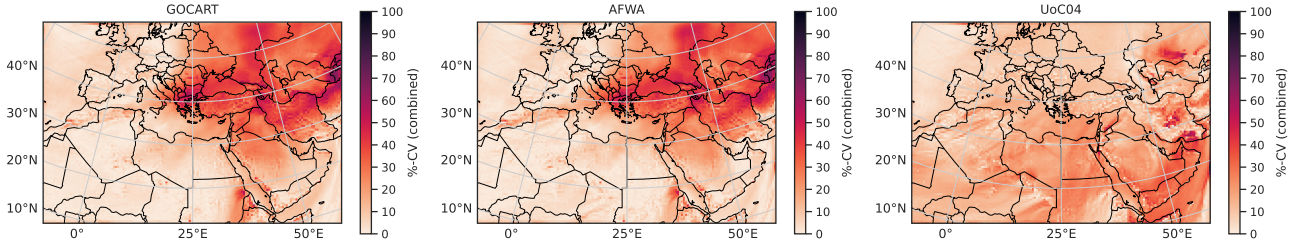

Figure A3. Spatial distribution of the coefficient of variation (CV) of aerosol optical depth (AOD) computed from two WRF-Chem simulations performed at 50 km and 10 km horizontal resolution for the different emission schemes (left: GOCART–CLM4, middle: AFWA–CLM4, right: UoC–CLM4). The CV is calculated as the standard deviation of the local difference between the two simulations normalized by its mean (upscaled in the finer resolution) and expressed as a percentage.

https://doi.org/10.5194/egusphere-2026-1900
Preprint. Discussion started: 19 June 2026

Table A1. AERONET station-wise AOD error statistics for different dust emission schemes (AFWA, GOCART, UoC04) and land-surface models (CLM4, Noah-MP).

	AFWA–CLM4				AFWA–Noah-MP				GOCART–CLM4				GOCART–Noah-MP				UoC04–CLM4				UoC04–Noah-MP			
Station	MBE	MAE	NMB%	NME%	MBE	MAE	NMB%	NME%	MBE	MAE	NMB%	NME%	MBE	MAE	NMB%	NME%	MBE	MAE	NMB%	NME%	MBE	MAE	NMB%	NME%
AgiaMarina Xyliatou	-0.09	0.27	-20.56	59.62	-0.07	0.26	-15.03	59.32	-0.09	0.26	-19.31	58.38	-0.1	0.26	-21.55	57.49	-0.27	0.33	-60.08	74.6	-0.17	0.31	-37.46	70.2
Antikythera_NOA	-0.03	0.2	-8.71	51.76	0.01	0.2	1.56	54.11	-0.02	0.2	-5.71	53.99	-0.03	0.2	-7.95	53.28	-0.26	0.28	-69.7	73.18	-0.14	0.22	-36.66	58.68
Aras_de_los_Olmos	-0.62	0.64	-85.94	88.65	-0.62	0.63	-85.96	87.92	-0.63	0.64	-87.14	88.9	-0.63	0.64	-87.86	89.3	-0.65	0.66	-90.64	91.5	-0.6	0.62	-83.28	86.43
Banizoumbou	-0.15	0.27	-26.67	46.57	-0.13	0.26	-21.91	45.68	-0.07	0.27	-12.81	46.38	-0.11	0.27	-19.7	46.31	-0.16	0.38	-27.37	66.32	-0.17	0.34	-29.36	58.97
Ben_Salem	-0.09	0.15	-20.38	34.11	-0.04	0.17	-8.19	37.5	-0.11	0.16	-23.67	35.06	-0.11	0.16	-23.57	34.9	-0.31	0.31	-69.24	69.33	-0.18	0.25	-39.26	55.96
Cabo_da_Roca	-0.33	0.35	-74.57	78.91	-0.33	0.34	-74.41	77.13	-0.34	0.36	-76.97	79.81	-0.35	0.36	-78.87	80.87	-0.37	0.37	-83.39	84.06	-0.31	0.33	-69.68	74.67
Cerro_Poyos	-0.11	0.27	-23.19	56.93	-0.12	0.25	-26.66	54.08	-0.18	0.25	-38.17	53.76	-0.18	0.25	-38.37	54.17	-0.21	0.29	-44.61	61.3	-0.02	0.34	-4.65	72.35
Eilat	-0.23	0.23	-65.5	65.6	-0.19	0.2	-55.33	56.41	-0.21	0.21	-59.94	60.3	-0.2	0.2	-58.06	58.42	-0.29	0.29	-83.02	83.02	-0.21	0.22	-61.23	63.9
El_Arenosillo	-0.27	0.37	-51.72	71.1	-0.28	0.35	-54.91	67.82	-0.31	0.35	-60.57	68.57	-0.32	0.36	-62.37	69.01	-0.33	0.42	-63.87	81.88	-0.22	0.4	-41.81	78.03
Ersa	-0.32	0.34	-64.19	68.16	-0.31	0.33	-62	65.51	-0.32	0.34	-64.99	68.33	-0.33	0.34	-66.51	69.2	-0.41	0.41	-82.24	82.37	-0.31	0.35	-62.4	70.05
Finokalia-FKL	-0.1	0.25	-24.03	58.9	-0.07	0.26	-16.84	60.33	-0.09	0.25	-21.55	59.21	-0.1	0.25	-23.7	58.6	-0.3	0.33	-70.3	77.63	-0.21	0.29	-48.09	67.83
Guadiana-UGR	-0.3	0.37	-56.26	70.04	-0.32	0.37	-59.35	68.47	-0.33	0.37	-62.78	69.11	-0.34	0.37	-64.57	69.64	-0.4	0.43	-74.37	80.18	-0.3	0.39	-56.55	73.85
IER_Cinzana	-0.14	0.25	-26.18	47.32	-0.08	0.26	-15.3	48.32	-0.14	0.25	-25.6	46.97	-0.16	0.25	-30.99	47.42	-0.25	0.37	-47.73	70.49	-0.24	0.32	-44.86	60.94
IMAA_Potenza	-0.28	0.36	-50.72	63.81	-0.26	0.35	-46.89	63.34	-0.29	0.36	-51.13	63.89	-0.29	0.36	-52.21	64.02	-0.46	0.46	-82.36	82.39	-0.34	0.4	-61.39	71.14
IMS-METU-ERDEMLI	-0.41	0.51	-53.1	65.13	-0.38	0.49	-49.29	62.78	-0.42	0.5	-53.9	63.96	-0.43	0.5	-54.96	64.25	-0.61	0.67	-78.71	86.66	-0.51	0.62	-66.19	79.73
Lampedusa	-0.12	0.22	-25.48	45.2	-0.09	0.22	-18.66	44.42	-0.12	0.22	-24.61	45.38	-0.12	0.22	-25.67	44.93	-0.35	0.36	-71.33	73.65	-0.22	0.29	-45.58	60.13
Medenine-IRA	-0.04	0.17	-8.23	38.6	0.02	0.19	5.4	43	-0.01	0.17	-1.65	37.93	-0.01	0.17	-1.67	37.74	-0.27	0.31	-60.41	70.2	-0.06	0.28	-14.51	64.8
Mezaira	0.01	0.25	2.16	53.43	0.08	0.29	18.19	61.53	-0.06	0.19	-12.56	39.94	-0.03	0.18	-6.36	39.67	0	0.37	-0.7	78.85	0.43	0.71	91.74	151.83
Momuy_MF	-0.68	0.69	-90.84	92.38	-0.67	0.68	-89.89	91.01	-0.68	0.68	-90.63	91.53	-0.68	0.69	-91.38	92.23	-0.7	0.7	-93.77	93.77	-0.65	0.66	-87.08	87.82
Montsec	-0.4	0.49	-66.42	82.6	-0.41	0.48	-69.21	80.12	-0.43	0.48	-71.18	80.62	-0.44	0.48	-73.14	80.72	-0.5	0.51	-83.75	85.79	-0.46	0.49	-76.26	81.07
OHP_OBSERVATOIRE	-0.49	0.53	-75.13	81.75	-0.49	0.52	-74.92	80.34	-0.5	0.53	-76.63	80.91	-0.51	0.53	-78.24	81.75	-0.55	0.56	-85	85.47	-0.47	0.52	-72.67	79.28
SEDE_BOKER	-0.09	0.2	-24.4	54.12	-0.04	0.2	-10.88	54.06	-0.05	0.19	-14.36	52.17	-0.05	0.19	-14.18	50.94	-0.19	0.26	-51.64	70.45	-0.12	0.22	-31.65	59.83
Saada	-0.19	0.29	-44.4	68.65	-0.2	0.27	-47.44	64.06	-0.24	0.27	-56.84	63.18	-0.24	0.27	-56.74	63.84	-0.23	0.37	-53.12	86.63	-0.19	0.34	-44.68	79.37
Tabernas_PSA-DLR	-0.23	0.31	-46.72	61.71	-0.24	0.3	-48.65	59.88	-0.27	0.31	-54.12	61.32	-0.28	0.31	-55.64	61.92	-0.34	0.37	-69.05	73.66	-0.24	0.34	-48.18	69.08
Average	-0.24	0.33	-42.97	62.71	-0.22	0.33	-38.61	61.96	-0.25	0.33	-44.45	61.23	-0.25	0.33	-45.59	61.28	-0.35	0.41	-66.52	78.47	-0.25	0.39	-44.66	74.00

https://doi.org/10.5194/egusphere-2026-1900
Preprint. Discussion started: 19 June 2026

Table A2. EMEP station-wise $PM_{10} - PM_{2.5}$ error statistics for different dust emission schemes (AFWA, GOCART, UoC04) and land-surface models (CLM4, Noah-MP).

	AFWA–CLM4				AFWA–Noah-MP				GOCART–CLM4				GOCART–Noah-MP				UoC04–CLM4				UoC04–Noah-MP			
Station	MBE	MAE	NMB%	NME%	MBE	MAE	NMB%	NME%	MBE	MAE	NMB%	NME%	MBE	MAE	NMB%	NME%	MBE	MAE	NMB%	NME%	MBE	MAE	NMB%	NME%
AT0002R	1.89	5.60	50.61	149.72	2.74	6.19	73.16	165.66	2.14	5.72	57.30	153.01	1.59	5.30	42.55	141.67	-2.38	3.18	-63.62	85.01	-0.89	3.56	-23.82	95.12
CH0002R	3.06	5.94	89.70	174.10	3.59	6.31	105.21	184.73	3.80	6.53	111.25	191.33	3.25	6.10	95.09	178.70	-1.54	3.34	-45.17	97.79	0.18	4.13	5.29	121.01
CH0005R	3.13	5.22	101.37	169.02	3.56	5.61	115.30	181.73	3.85	5.82	124.88	188.59	3.34	5.40	108.08	174.79	-1.43	3.01	-46.48	97.53	0.03	3.77	0.89	122.03
CY0002R	7.32	11.72	77.33	123.74	12.07	14.98	127.43	158.25	12.60	15.87	133.08	167.65	11.88	15.38	125.45	162.49	-5.19	6.99	-54.85	73.85	0.36	8.37	3.83	88.37
CZ0003R	-0.85	5.87	-16.00	111.19	-0.26	6.14	-4.98	116.33	-0.68	5.82	-12.86	110.26	-1.16	5.56	-22.02	105.37	-3.87	4.97	-73.31	94.06	-2.52	5.28	-47.73	100.02
DE0002R	0.45	4.10	13.51	122.38	1.04	4.30	31.06	128.52	0.63	4.13	18.89	123.39	0.11	3.90	3.27	116.64	-1.16	3.00	-34.76	89.50	1.00	4.11	29.83	122.70
DE0003R	1.10	5.16	26.19	123.03	1.75	5.60	41.59	133.49	1.67	5.60	39.69	133.29	1.17	5.25	27.95	125.07	-2.67	4.11	-63.53	97.97	-1.19	4.68	-28.25	111.39
DE0007R	-0.99	5.15	-20.79	108.49	-0.42	5.31	-8.77	111.82	-0.90	5.05	-18.99	106.35	-1.35	4.91	-28.48	103.39	-2.94	4.14	-61.85	87.19	-1.13	4.78	-23.73	100.64
DE0008R	1.58	4.04	60.12	153.39	2.11	4.36	80.33	165.78	1.81	4.20	68.83	159.67	1.36	3.87	51.63	147.26	-1.07	2.60	-40.62	98.94	0.48	3.43	18.11	130.51
DE0044R	-0.90	5.26	-18.34	107.69	-0.40	5.32	-8.16	109.01	-0.72	5.24	-14.79	107.40	-1.24	4.99	-25.44	102.14	-3.18	4.39	-65.23	89.98	-1.54	4.73	-31.61	96.99
ES0001R	4.27	8.14	67.16	128.13	4.64	8.09	73.13	127.30	4.70	8.76	73.98	137.84	3.81	8.08	59.98	127.20	-1.79	6.04	-28.11	95.12	2.48	8.27	38.98	130.19
ES0006R	0.71	9.78	5.65	78.11	2.48	10.07	19.80	80.40	1.56	10.14	12.49	80.96	0.56	9.95	4.47	79.43	-7.78	7.97	-62.16	63.61	-3.02	6.03	-24.14	48.11
ES0007R	7.05	10.96	91.46	142.14	7.46	10.86	96.85	140.86	7.92	11.69	102.80	151.72	6.69	10.68	86.85	138.59	-3.63	6.82	-47.14	88.52	-0.03	8.53	-0.44	110.72
ES0008R	-0.34	8.50	-4.22	105.80	-0.09	7.76	-1.06	96.61	0.26	8.52	3.24	106.03	-0.66	8.13	-8.19	101.22	-4.33	5.98	-53.96	74.46	-0.58	7.00	-7.25	87.15
ES0009R	5.65	8.93	97.32	153.67	5.44	8.39	93.59	144.39	6.19	9.38	106.51	161.49	5.19	8.56	89.31	147.27	-2.61	4.97	-44.84	85.52	0.62	6.22	10.64	107.00
ES0010R	-0.19	7.11	-2.53	95.96	0.71	7.23	9.55	97.61	0.59	7.42	7.96	100.16	-0.06	7.16	-0.85	96.65	-4.43	5.60	-59.78	75.59	-1.43	5.61	-19.25	75.77
ES0011R	5.62	8.69	114.68	177.43	5.98	8.58	122.13	175.20	6.20	9.00	126.55	183.78	5.17	8.23	105.64	168.06	-0.60	4.44	-12.32	90.70	4.56	7.95	93.11	162.36
ES0014R	4.64	9.16	64.84	127.94	5.69	9.52	79.42	133.01	5.11	9.40	71.32	131.24	3.95	8.70	55.16	121.55	-3.94	5.71	-55.05	79.83	-0.71	6.37	-9.85	89.03
ES0016R	5.36	6.62	200.96	248.40	5.61	6.64	210.31	249.10	5.94	7.04	222.98	264.19	4.94	6.20	185.19	232.52	1.35	3.08	50.57	115.45	5.17	6.31	193.93	236.82
ES1778R	1.38	1.62	239.70	282.19	1.70	1.89	295.64	328.34	2.01	2.22	349.86	386.75	1.76	2.01	306.46	348.92	0.98	1.17	169.74	203.71	2.64	2.64	459.89	459.89
FR0008R	2.33	4.86	80.23	167.21	2.95	5.37	101.33	184.61	2.84	5.32	97.75	183.01	2.26	4.87	77.72	167.56	-0.78	3.59	-26.67	123.47	1.28	5.01	44.11	172.14
FR0009R	-0.52	5.90	-10.09	114.59	0.16	6.10	3.11	118.49	-0.31	5.91	-6.06	114.87	-0.93	5.59	-18.09	108.58	-2.41	5.17	-46.85	100.41	0.41	6.77	8.06	131.44
FR0010R	2.20	6.77	47.62	146.59	3.02	7.24	65.33	156.77	2.54	6.95	55.04	150.43	1.84	6.43	39.84	139.16	-1.67	5.18	-36.13	112.05	1.45	7.22	31.29	156.25
FR0013R	4.77	7.23	129.52	196.12	5.21	7.41	141.29	201.03	5.52	7.83	149.62	212.30	4.49	6.96	121.78	188.84	0.22	4.35	5.95	118.12	3.88	7.07	105.38	191.68
FR0015R	1.25	6.66	23.90	127.34	2.38	7.32	45.47	139.97	1.75	6.96	33.41	133.22	0.79	6.28	15.19	120.08	0.06	6.41	1.07	122.61	5.75	10.85	109.94	207.64
FR0018R	1.86	4.96	62.92	167.69	2.84	5.66	95.86	191.11	2.23	5.24	75.24	176.85	1.50	4.68	50.81	158.13	1.39	5.00	47.01	169.02	6.08	8.96	205.38	302.63
FR0023R	3.61	5.83	106.82	172.42	4.04	6.20	119.37	183.36	4.34	6.53	128.40	192.94	3.65	6.01	107.82	177.67	-1.39	3.65	-41.14	107.84	0.58	4.76	17.13	140.83
FR0028R	1.32	5.04	36.10	137.38	2.75	6.06	74.94	165.10	1.88	5.47	51.20	149.08	1.15	4.96	31.23	135.04	1.89	6.12	51.44	166.66	7.94	11.28	216.27	307.19
GB1055R	-0.73	4.32	-18.28	108.55	0.53	5.08	13.21	127.53	-0.34	4.61	-8.46	115.61	-0.81	4.37	-20.36	109.59	-0.07	5.23	-1.67	131.28	4.28	8.70	107.42	218.42
GR0001R	7.10	13.08	74.57	137.47	12.32	17.17	129.41	180.39	10.50	16.39	110.28	172.20	9.31	15.43	97.85	162.13	-6.80	7.56	-71.42	79.39	-2.95	7.53	-31.02	79.15
HR0002R	-1.50	8.12	-20.17	108.89	-0.36	8.73	-4.83	117.08	-0.86	8.53	-11.48	114.35	-1.44	8.21	-19.35	110.08	-5.78	6.50	-77.58	87.11	-3.92	6.66	-52.60	89.32
HU0017R	2.26	4.83	74.85	159.64	3.70	6.05	122.52	200.09	2.56	5.13	84.67	169.71	2.02	4.68	66.69	154.90	-1.66	2.98	-54.99	98.51	0.04	3.49	1.35	115.46
IT0019R	7.90	10.85	144.13	197.87	10.26	12.99	187.14	236.91	9.46	12.28	172.48	223.93	8.32	11.28	151.69	205.68	-2.31	4.87	-42.15	88.71	1.01	6.35	18.36	115.73
LV0010R	-5.47	8.68	-57.83	91.78	-3.64	9.52	-38.44	100.68	-5.48	8.69	-57.92	91.90	-6.06	8.61	-64.07	90.99	-6.23	8.78	-65.83	92.78	-2.54	10.49	-26.84	110.87
NL0009R	-5.82	9.16	-58.35	91.83	-4.77	8.95	-47.82	89.75	-5.53	8.89	-55.47	89.12	-6.19	8.88	-62.08	89.08	-6.30	8.22	-63.15	82.45	-2.47	8.87	-24.74	88.95
NL0010R	-5.68	10.76	-53.82	101.84	-5.13	10.54	-48.54	99.77	-5.53	10.54	-52.32	99.76	-6.29	10.30	-59.55	97.48	-7.70	9.73	-72.88	92.16	-4.82	10.70	-45.61	101.30
NL0091R	-5.36	9.07	-53.56	90.60	-4.20	8.85	-41.91	88.38	-5.17	8.76	-51.61	87.49	-5.90	8.74	-58.88	87.33	-6.01	8.00	-60.00	79.86	-1.69	9.03	-16.87	90.14
NL0644R	-6.65	10.18	-60.37	92.39	-5.66	10.02	-51.40	91.00	-6.42	9.98	-58.31	90.60	-7.12	9.94	-64.62	90.24	-7.43	9.56	-67.47	86.82	-3.67	10.47	-33.32	95.10
PL0005R	-0.07	4.42	-1.89	116.39	1.18	5.25	31.16	138.15	-0.34	3.99	-8.89	104.83	-0.76	3.84	-20.11	100.98	-2.49	3.09	-65.41	81.20	-1.06	3.52	-27.95	92.47
PL0009R	-3.27	7.10	-46.05	100.07	-2.14	7.54	-30.14	106.26	-3.47	6.45	-48.91	90.88	-3.87	6.41	-54.57	90.39	-5.54	6.02	-78.17	84.90	-3.82	6.13	-53.89	86.35
SI0008R	6.13	7.78	222.42	282.28	7.60	9.10	275.52	329.95	6.71	8.26	243.33	299.61	6.05	7.65	219.21	277.56	-1.13	2.43	-40.85	87.99	0.81	3.13	29.25	113.41
Average	1.36	7.15	45.40	141.26	2.40	7.67	65.71	153.04	1.99	7.57	59.20	151.41	1.28	7.13	43.91	140.99	-2.79	5.22	-36.57	99.46	0.27	6.55	29.74	136.64

Author contributions. Investigation, Formal Analysis, Writing – Original Draft: SD, EL, AV, TC. Data Curation: AV, EL, PK. Visualisation: AV, SD, EL, PK. Writing – Review & Editing: All authors. Conceptualisation, Supervision, Funding Acquisition: TC.

Competing interests. The authors declare no competing interests.

Acknowledgements. This study was supported by funding from the European Union's Horizon Europe Research and Innovation Programme under the Marie Skłodowska-Curie grant agreement No. 101168425 (Dust-DN), and under grant agreement No. 856612 (EMME-CARE) and the Cyprus Government, and the Cyprus Research and Innovation Foundation (Project ID: COM-CONCEPT-ENERGY/0624) .

https://doi.org/10.5194/egusphere-2026-1900
Preprint. Discussion started: 19 June 2026

References

Banks, J. R., Heinold, B., and Schepanski, K.: Impacts of the Desiccation of the Aral Sea on the Central Asian Dust Life-Cycle, Journal of Geophysical Research: Atmospheres, 127, e2022JD036 618, https://doi.org/https://doi.org/10.1029/2022JD036618, e2022JD036618 2022JD036618, 2022.

Bessonova, V., Tapoglou, E., Dorrell, R., Dethlefs, N., and York, K.: Global evaluation of wave data reanalysis: Comparison of the ERA5 dataset to buoy observations, Applied Ocean Research, 157, 104 490, https://doi.org/https://doi.org/10.1016/j.apor.2025.104490, 2025.

Bukowski, J. and van den Heever, S. C.: The Impact of Land Surface Properties on Haboobs and Dust Lofting, Journal of the Atmospheric Sciences, 79, 3195 – 3218, https://doi.org/10.1175/JAS-D-22-0001.1, 2022.

Cenlin_He, Barlage, M., Valayamkunnath, P., Gill, D., Mocko, D., and Chen, F.: NCAR/noahmp: Release of v5.0.0, https://doi.org/10.5281/zenodo.7901855, 2023.

Chen, S., Huang, J., Zhao, C., Qian, Y., Leung, L. R., and Yang, B.: Modeling the transport and radiative forcing of Taklimakan dust over the Tibetan Plateau: A case study in the summer of 2006, Journal of Geophysical Research: Atmospheres, 118, 797–812, https://doi.org/https://doi.org/10.1002/jgrd.50122, 2013.

Chin, M., Rood, R. B., Lin, S.-J., Müller, J.-F., and Thompson, A. M.: Atmospheric sulfur cycle simulated in the global model GOCART: Model description and global properties, Journal of Geophysical Research: Atmospheres, 105, 24 671–24 687, https://doi.org/https://doi.org/10.1029/2000JD900384, 2000.

Deb, S., Louca, E., Violaris, A., Kiriakidis, P., Proestos, Y., Kushta, J., Gkikas, A., Pozzer, A., and Christoudias, T.: Data and model configuration for manuscript "Evaluation of WRF-Chem (version 4.7.1) aeolian dust emission and land surface models over the dust belt", https://doi.org/10.5281/zenodo.19498593, 2026.

Flaounas, E., Kotroni, V., Lagouvardos, K., Klose, M., Flamant, C., and Giannaros, T. M.: Sensitivity of the WRF-Chem (V3.6.1) model to different dust emission parametrisation: assessment in the broader Mediterranean region, Geoscientific Model Development, 10, 2925–2945, https://doi.org/10.5194/gmd-10-2925-2017, 2017.

Fountoukis, C., Ackermann, L., Ayoub, M., Gladich, I., Hoehn, R., and Skillern, A.: Impact of atmospheric dust emission schemes on dust production and concentration over the Arabian Peninsula, Modeling Earth Systems and Environment, 2, https://doi.org/10.1007/s40808-016-0181-z, 2016.

Freitas, S. R., Grell, G. A., and Li, H.: The Grell–Freitas (GF) convection parameterization: recent developments, extensions, and applications, Geoscientific Model Development, 14, 5393–5411, https://doi.org/10.5194/gmd-14-5393-2021, 2021.

Georgiou, G. K., Christoudias, T., Proestos, Y., Kushta, J., Pikridas, M., Sciare, J., Savvides, C., and Lelieveld, J.: Evaluation of WRF-Chem model (v3.9.1.1) real-time air quality forecasts over the Eastern Mediterranean, Geoscientific Model Development, 15, 4129–4146, 2022.

Giannadaki, D., Pozzer, A., and Lelieveld, J.: Modeled global effects of airborne desert dust on air quality and premature mortality, Atmospheric Chemistry and Physics, 14, 957–968, https://doi.org/10.5194/acp-14-957-2014, 2014.

Giles, D. M., Sinyuk, A., Sorokin, M. G., Schafer, J. S., Smirnov, A., Slutsker, I., Eck, T. F., Holben, B. N., Lewis, J. R., Campbell, J. R., Welton, E. J., Korkin, S. V., and Lyapustin, A. I.: Advancements in the Aerosol Robotic Network (AERONET) Version 3 database – automated near-real-time quality control algorithm with improved cloud screening for Sun photometer aerosol optical depth (AOD) measurements, Atmospheric Measurement Techniques, 12, 169–209, https://doi.org/10.5194/amt-12-169-2019, 2019.

Gillett, D. and Morales, C.: Environmental factors affecting dust emission by wind erosion, Saharan dust, pp. 71–94, 1979.

https://doi.org/10.5194/egusphere-2026-1900
Preprint. Discussion started: 19 June 2026

Gillette, D. A. and Passi, R.: Modeling dust emission caused by wind erosion, Journal of Geophysical Research: Atmospheres, 93, 14 233–14 242, 1988.

Ginoux, P., Chin, M., Tegen, I., Prospero, J., Holben, B., Dubovik, O., and Lin, S.-J.: Sources and distributions of dust aerosols simulated with the GOCART model, Journal of Geophysical Research, 106, 20 255–20 274, https://doi.org/10.1029/2000JD000053, 2001.

Gkikas, A., Proestakis, E., Amiridis, V., Kazadzis, S., Di Tomaso, E., Tsekeri, A., Marinou, E., Hatzianastassiou, N., and Pérez García-Pando, C.: ModIs Dust AeroSol (MIDAS): a global fine-resolution dust optical depth data set, Atmospheric Measurement Techniques, 14, 309–334, https://doi.org/10.5194/amt-14-309-2021, 2021.

Gkikas, A., Proestakis, E., Amiridis, V., Kazadzis, S., Di Tomaso, E., Marinou, E., Hatzianastassiou, N., Kok, J. F., and García-Pando, C. P.: Quantification of the dust optical depth across spatiotemporal scales with the MIDAS global dataset (2003–2017), Atmospheric Chemistry and Physics, 22, 3553–3578, https://doi.org/10.5194/acp-22-3553-2022, 2022.

Grell, G. A., Peckham, S. E., Schmitz, R., McKeen, S. A., Frost, G., Skamarock, W. C., and Eder, B.: Fully coupled "online" chemistry within the WRF model, Atmospheric Environment, 39, 6957–6975, https://doi.org/https://doi.org/10.1016/j.atmosenv.2005.04.027, 2005.

Griffin, D. W.: Atmospheric Movement of Microorganisms in Clouds of Desert Dust and Implications for Human Health, Clinical Microbiology Reviews, 20, 459–477, https://doi.org/10.1128/cmr.00039-06, 2007.

Gualtieri, G.: Reliability of ERA5 Reanalysis Data for Wind Resource Assessment: A Comparison against Tall Towers, Energies, 14, https://doi.org/10.3390/en14144169, 2021.

He, C., Valayamkunnath, P., Barlage, M., Chen, F., Gochis, D., Cabell, R., Schneider, T., Rasmussen, R., Niu, G.-Y., Yang, Z.-L., Niyogi, D., and Ek, M.: Modernizing the open-source community Noah with multi-parameterization options (Noah-MP) land surface model (version 5.0) with enhanced modularity, interoperability, and applicability, Geoscientific Model Development, 16, 5131–5151, https://doi.org/10.5194/gmd-16-5131-2023, 2023.

Holben, B., Eck, T., Slutsker, I., Tanré, D., Buis, J., Setzer, A., Vermote, E., Reagan, J., Kaufman, Y., Nakajima, T., Lavenu, F., Jankowiak, I., and Smirnov, A.: AERONET—A Federated Instrument Network and Data Archive for Aerosol Characterization, Remote Sensing of Environment, 66, 1–16, https://doi.org/https://doi.org/10.1016/S0034-4257(98)00031-5, 1998.

Hong, S.-Y., Noh, Y., and Dudhia, J.: A new vertical diffusion package with an explicit treatment of entrainment processes., Monthly Weather Review, 134, 2318–2341, https://doi.org/10.1175/MWR3199.1, 2006.

Indoitu, R., Kozhoridze, G., Batyrbaeva, M., Vitkovskaya, I., Orlovsky, N., Blumberg, D., and Orlovsky, L.: Dust emission and environmental changes in the dried bottom of the Aral Sea, Aeolian Research, 17, 101–115, https://doi.org/https://doi.org/10.1016/j.aeolia.2015.02.004, 2015.

Kiriakidis, P., Gkikas, A., Papangelis, G., Christoudias, T., Kushta, J., Proestakis, E., Kampouri, A., Marinou, E., Drakaki, E., Benedetti, A., Rennie, M., Retscher, C., Straume, A. G., Dandocsi, A., Sciare, J., and Amiridis, V.: The impact of using assimilated Aeolus wind data on regional WRF-Chem dust simulations, Atmospheric Chemistry and Physics, 23, 4391–4417, https://doi.org/10.5194/acp-23-4391-2023, 2023.

Kok, J., Parteli, E., Michaels, T., and Francis, D.: The physics of wind-blown sand and dust, Reports on progress in physics. Physical Society (Great Britain), 75, 106 901, https://doi.org/10.1088/0034-4885/75/10/106901, 2012.

Kok, J. F., Adebiyi, A. A., Albani, S., Balkanski, Y., Checa-Garcia, R., Chin, M., Colarco, P. R., Hamilton, D. S., Huang, Y., Ito, A., Klose, M., Leung, D. M., Li, L., Mahowald, N. M., Miller, R. L., Obiso, V., Pérez García-Pando, C., Rocha-Lima, A., Wan, J. S., and Whicker, C. A.: Improved representation of the global dust cycle using observational constraints on dust properties and abundance, Atmospheric Chemistry and Physics, 21, 8127–8167, https://doi.org/10.5194/acp-21-8127-2021, 2021a.

https://doi.org/10.5194/egusphere-2026-1900
Preprint. Discussion started: 19 June 2026

Kok, J. F., Adebiyi, A. A., Albani, S., Balkanski, Y., Checa-Garcia, R., Chin, M., Colarco, P. R., Hamilton, D. S., Huang, Y., Ito, A., Klose, M., Li, L., Mahowald, N. M., Miller, R. L., Obiso, V., Pérez García-Pando, C., Rocha-Lima, A., and Wan, J. S.: Contribution of the world's main dust source regions to the global cycle of desert dust, Atmospheric Chemistry and Physics, 21, 8169–8193, https://doi.org/10.5194/acp-21-8169-2021, 2021b.

Lawrence, D. M., Oleson, K. W., Flanner, M. G., Thornton, P. E., Swenson, S. C., Lawrence, P. J., Zeng, X., Yang, Z.-L., Levis, S., Sakaguchi, K., Bonan, G. B., and Slater, A. G.: Parameterization improvements and functional and structural advances in Version 4 of the Community Land Model, Journal of Advances in Modeling Earth Systems, 3, https://doi.org/https://doi.org/10.1029/2011MS00045, 2011.

Lee, J.-H. and Lee, S.-H.: Modeling a severe wintertime Asian dust event observed in the East Asia region: Sensitivity of the WRF-Chem dust emission schemes, Atmospheric Pollution Research, 13, 101 599, https://doi.org/https://doi.org/10.1016/j.apr.2022.101599, 2022.

LeGrand, S. L., Polashenski, C., Letcher, T. W., Creighton, G. A., Peckham, S. E., and Cetola, J. D.: The AFWA dust emission scheme for the GOCART aerosol model in WRF-Chem v3. 8.1, Geoscientific Model Development, 12, 131–166, 2019.

Mahowald, N. M., Kloster, S., Engelstaedter, S., Moore, J. K., Mukhopadhyay, S., McConnell, J. R., Albani, S., Doney, S. C., Bhattacharya, A., Curran, M. A. J., Flanner, M. G., Hoffman, F. M., Lawrence, D. M., Lindsay, K., Mayewski, P. A., Neff, J., Rothenberg, D., Thomas, E., Thornton, P. E., and Zender, C. S.: Observed 20th century desert dust variability: impact on climate and biogeochemistry, Atmospheric Chemistry and Physics, 10, 10 875–10 893, https://doi.org/10.5194/acp-10-10875-2010, 2010.

Marticorena, B. and Bergametti, G.: Modeling the atmospheric dust cycle: 1. Design of a soil-derived dust emission scheme, Journal of Geophysical Research: Atmospheres, 100, 16 415–16 430, https://doi.org/https://doi.org/10.1029/95JD00690, 1995.

Miller, R. L., Tegen, I., and Perlwitz, J. P.: Surface radiative forcing by soil dust aerosols and the hydrologic cycle, Journal of Geophysical Research, 109, D04 203, https://doi.org/10.1029/2003JD004085, 2004.

Mlawer, E. J., Taubman, S. J., Brown, P. D., Iacono, M. J., and Clough, S. A.: Radiative transfer for inhomogeneous atmosphers: RRTM, a validated correlated0k model for the long-wave, J. Geophys. Res., 102, 16 663–16 682, https://doi.org/https://doi.org/10.1029/97JD00237, 1997.

Najafpour, N., Afshin, H., and Firoozabadi, B.: Sensitivity study and comparative evaluation of WRF-Chem over Iran: Available and embedded dust emission schemes, Atmospheric Pollution Research, 14, 101 930, https://doi.org/https://doi.org/10.1016/j.apr.2023.101930, 2023.

Niu, G.-Y., Yang, Z.-L., Mitchell, K. E., Chen, F., Ek, M. B., Barlage, M., Kumar, A., Manning, K., Niyogi, D., Rosero, E., Tewari, M., and Xia, Y.: The community Noah land surface model with multiparameterization options (Noah-MP): 1. Model description and evaluation with local-scale measurements, Journal of Geophysical Research: Atmospheres, 116, https://doi.org/https://doi.org/10.1029/2010JD015139, 2011.

Pikridas, M., Vrekoussis, M., Sciare, J., Kleanthous, S., Vasiliadou, E., Kizas, C., Savvides, C., and Mihalopoulos, N.: Spatial and temporal (short and long-term) variability of submicron, fine and sub-10μm particulate matter (PM1, PM2.5, PM10) in Cyprus, Atmospheric Environment, 191, 79–93, https://doi.org/https://doi.org/10.1016/j.atmosenv.2018.07.048, 2018.

Prospero, J. M., Ginoux, P., Torres, O., Nicholson, S. E., and Gill, T. E.: ENVIRONMENTAL CHARACTERIZATION OF GLOBAL SOURCES OF ATMOSPHERIC SOIL DUST IDENTIFIED WITH THE NIMBUS 7 TOTAL OZONE MAPPING SPECTROMETER (TOMS) ABSORBING AEROSOL PRODUCT, Reviews of Geophysics, 40, 2–1–2–31, https://doi.org/https://doi.org/10.1029/2000RG000095, 2002.

https://doi.org/10.5194/egusphere-2026-1900
Preprint. Discussion started: 19 June 2026

Pérez, C., Nickovic, S., Baldasano, J. M., Sicard, M., Rocadenbosch, F., and Cachorro, V. E.: A long Saharan dust event over the western Mediterranean: Lidar, Sun photometer observations, and regional dust modeling, Journal of Geophysical Research: Atmospheres, 111, https://doi.org/https://doi.org/10.1029/2005JD006579, 2006.

Rizza, U., Miglietta, M. M., Mangia, C., Ielpo, P., Morichetti, M., Iachini, C., Virgili, S., and Passerini, G.: Sensitivity of WRF-Chem model to land surface schemes: Assessment in a severe dust outbreak episode in the Central Mediterranean (Apulia Region), Atmospheric Research, 201, 168–180, https://doi.org/https://doi.org/10.1016/j.atmosres.2017.10.022, 2018.

Sciare, J., Bardouki, H., Moulin, C., and Mihalopoulos, N.: Aerosol sources and their contribution to the chemical composition of aerosols in the Eastern Mediterranean Sea during summertime, Atmospheric Chemistry and Physics, 3, 291–302, https://doi.org/10.5194/acp-3-291-2003, 2003.

Shao, Y.: A model for mineral dust emission, Journal of Geophysical Research: Atmospheres, 106, 20 239–20 254, https://doi.org/https://doi.org/10.1029/2001JD900171, 2001.

Shao, Y.: Simplification of a dust emission scheme and comparison with data, Journal of Geophysical Research: Atmospheres, 109, https://doi.org/https://doi.org/10.1029/2003JD004372, 2004.

Shao, Y., Ishizuka, M., Mikami, M., and Leys, J. F.: Parameterization of size-resolved dust emission and validation with measurements, Journal of Geophysical Research: Atmospheres, 116, https://doi.org/https://doi.org/10.1029/2010JD014527, 2011.

Su, L. and Fung, J. C. H.: Sensitivities of WRF-Chem to dust emission schemes and land surface properties in simulating dust cycles during springtime over East Asia, Journal of Geophysical Research: Atmospheres, 120, 11,215–11,230, https://doi.org/https://doi.org/10.1002/2015JD023446, 2015.

Tegen, I. and Fung, I.: Modeling of mineral dust transport in the atmosphere: Sources, transport, and optical thickness, Journal of Geophysical Research, 99, 22 897–22 914, https://doi.org/10.1029/94JD01928, 1994.

Wang, X., Jiang, L., Guo, Z., Xie, X., Li, L., Gong, K., and Hu, J.: Influence of meteorological reanalysis field on air quality modeling in the Yangtze River Delta, China, Atmospheric Environment, 318, 120 231, https://doi.org/https://doi.org/10.1016/j.atmosenv.2023.120231, 2024.

Wu, S., Zheng, J., Zou, H., Wang, H., and Tao, L.: The influence of ERA5 and FNL driven WRF on sensitivity experiments of small-scale underlying surface changes: a case study of poyang lake in China, Journal of Atmospheric and Solar-Terrestrial Physics, 277, 106 650, https://doi.org/https://doi.org/10.1016/j.jastp.2025.106650, 2025.

Xi, X., Wang, J., Lu, Z., Sayer, A. M., Lee, J., Levy, R. C., Wang, Y., Lyapustin, A., Liu, H., Laszlo, I., Ahn, C., Torres, O., Abdullaev, S., Limbacher, J., and Kahn, R. A.: Analysis of a saline dust storm from the Aralkum Desert – Part 1: Consistency between multisensor satellite aerosol products, Atmospheric Chemistry and Physics, 25, 7403–7429, https://doi.org/10.5194/acp-25-7403-2025, 2025.

Yoon, J. W., Lee, S., Lee, E., and Park, S. K.: Evaluation of dust emission and land surface schemes in predicting a mega Asian dust storm over South Korea using WRF-Chem, Geoscientific Model Development, 18, 2303–2328, https://doi.org/10.5194/gmd-18-2303-2025, 2025.

Yuan, T., Chen, S., Huang, J., Zhang, X., Luo, Y., Ma, X., and Zhang, G.: Sensitivity of simulating a dust storm over Central Asia to different dust schemes using the WRF-Chem model, Atmospheric Environment, 207, 16–29, https://doi.org/https://doi.org/10.1016/j.atmosenv.2019.03.014, 2019.

Zhang, X., Zhao, L., Tong, D. Q., Wu, G., Dan, M., and Teng, B.: A Systematic Review of Global Desert Dust and Associated Human Health Effects, Atmosphere, 7, https://doi.org/10.3390/atmos7120158, 2016.

Zhao, A., Ryder, C. L., and Wilcox, L. J.: How well do the CMIP6 models simulate dust aerosols?, Atmospheric Chemistry and Physics, 22, 2095–2119, https://doi.org/10.5194/acp-22-2095-2022, 2022.

https://doi.org/10.5194/egusphere-2026-1900
Preprint. Discussion started: 19 June 2026

Zhao, J., Ma, X., Wu, S., and Sha, T.: Dust emission and transport in Northwest China: WRF-Chem simulation and comparisons with multi-sensor observations, Atmospheric Research, 241, 104 978, https://doi.org/https://doi.org/10.1016/j.atmosres.2020.104978, 2020.

Zittis, G., Hadjinicolaou, P., and Lelieveld, J.: Comparison of WRF Model Physics Parameterizations over the MENA-CORDEX Domain, American Journal of Climate Change, 03, 490–511, https://doi.org/10.4236/ajcc.2014.35042, 2014.